NASA/TM—2013-217855

Oxygen Permeability and Grain-Boundary Diffusion Applied to Alumina Scales

James L. Smialek and Nathan S. Jacobson
Glenn Research Center, Cleveland, Ohio

Brian Gleeson
University of Pittsburgh, Pittsburgh, Pennsylvania

David B. Hovis and Arthur H. Heuer
Case Western Reserve University, Cleveland, Ohio

August 2013

NASA STI Program . . . in Profile

Since its founding, NASA has been dedicated to the advancement of aeronautics and space science. The NASA Scientific and Technical Information (STI) program plays a key part in helping NASA maintain this important role.

The NASA STI Program operates under the auspices of the Agency Chief Information Officer. It collects, organizes, provides for archiving, and disseminates NASA's STI. The NASA STI program provides access to the NASA Aeronautics and Space Database and its public interface, the NASA Technical Reports Server, thus providing one of the largest collections of aeronautical and space science STI in the world. Results are published in both non-NASA channels and by NASA in the NASA STI Report Series, which includes the following report types:

- TECHNICAL PUBLICATION. Reports of completed research or a major significant phase of research that present the results of NASA programs and include extensive data or theoretical analysis. Includes compilations of significant scientific and technical data and information deemed to be of continuing reference value. NASA counterpart of peer-reviewed formal professional papers but has less stringent limitations on manuscript length and extent of graphic presentations.

- TECHNICAL MEMORANDUM. Scientific and technical findings that are preliminary or of specialized interest, e.g., quick release reports, working papers, and bibliographies that contain minimal annotation. Does not contain extensive analysis.

- CONTRACTOR REPORT. Scientific and technical findings by NASA-sponsored contractors and grantees.

- CONFERENCE PUBLICATION. Collected papers from scientific and technical conferences, symposia, seminars, or other meetings sponsored or cosponsored by NASA.

- SPECIAL PUBLICATION. Scientific, technical, or historical information from NASA programs, projects, and missions, often concerned with subjects having substantial public interest.

- TECHNICAL TRANSLATION. English-language translations of foreign scientific and technical material pertinent to NASA's mission.

Specialized services also include creating custom thesauri, building customized databases, organizing and publishing research results.

For more information about the NASA STI program, see the following:

- Access the NASA STI program home page at *http://www.sti.nasa.gov*

- E-mail your question to *help@sti.nasa.gov*

- Fax your question to the NASA STI Information Desk at 443–757–5803

- Phone the NASA STI Information Desk at 443–757–5802

- Write to:
  STI Information Desk
  NASA Center for AeroSpace Information
  7115 Standard Drive
  Hanover, MD 21076–1320

NASA/TM—2013-217855

Oxygen Permeability and Grain-Boundary Diffusion Applied to Alumina Scales

James L. Smialek and Nathan S. Jacobson
Glenn Research Center, Cleveland, Ohio

Brian Gleeson
University of Pittsburgh, Pittsburgh, Pennsylvania

David B. Hovis and Arthur H. Heuer
Case Western Reserve University, Cleveland, Ohio

National Aeronautics and
Space Administration

Glenn Research Center
Cleveland, Ohio 44135

August 2013

Acknowledgments

The following are acknowledged for their helpful discussions in the preparation of this manuscript: Dr. J.A. Nesbitt, Dr. T. Nakagawa, Dr. S. Kitaoka, and Dr. D. Naumenko. This work was supported by the NASA Fundamental Aeronautics Program and by the Office of Naval Research, Dr. David Shifler, Program Manager.

This work was sponsored by the Fundamental Aeronautics Program at the NASA Glenn Research Center.

Level of Review: This material has been technically reviewed by technical management.

Available from

NASA Center for Aerospace Information
7115 Standard Drive
Hanover, MD 21076–1320

National Technical Information Service
5301 Shawnee Road
Alexandria, VA 22312

Available electronically at http://www.sti.nasa.gov

Oxygen Permeability and Grain-Boundary Diffusion Applied to Alumina Scales

James L. Smialek and Nathan S. Jacobson
National Aeronautics and Space Administration
Glenn Research Center
Cleveland, Ohio 44135

Brian Gleeson
University of Pittsburgh
Pittsburgh, Pennsylvania 15260

David B. Hovis and Arthur H. Heuer
Case Western Reserve University
Cleveland, Ohio 44106

Summary

High-temperature oxygen permeability measurements had determined grain-boundary diffusivities (δD_{gb}) in bulk polycrystalline alumina in a recent study by Wada, Matsudaira, and Kitaoka. They predict that oxygen $\delta D_{gb,O}$ varies with oxygen pressure as $P_{O_2}^{-1/6}$ and dominates at low P_{O_2} whereas aluminum $\delta D_{gb,Al}$ varies with $P_{O_2}^{+3/16}$ and dominates at high P_{O_2}. In the present study, these relations enable detailed evaluations of alumina scale growth in terms of diffusivity and grain size. It is deduced that coupling these relations with a modified Wagner treatment for dominant inward oxygen growth produces the concise solution: $\Pi_i = k_{p,i} \cdot G_i = 12\ \delta D_{gb,O,int}$, where Π_i is a constant and $k_{p,i}$ and G_i refer to instantaneous values of the scale parabolic growth constant and grain size, respectively. To support this analysis, a commercial FeCrAl(Zr) alloy was oxidized at 1100 to 1400 °C to determine $k_{p,i}$, interfacial grain size, Π, and thus $\delta D_{gb,O,int}$. The $\delta D_{gb,O,int}$ values predicted from oxidation were 10 to 40 times less than those obtained by the above solution, but closer than extrapolations from typical high-temperature bulk measurements. Furthermore, the activation energy predicted from permeability relations for $\delta D_{gb,O,int}$ (298 kJ/mole) is shown here to be significantly lower than that predicted for bulk alumina (467 kJ/mole) under no P_{O_2} gradient. In comparison, the activation energy determined from oxidation was 375 kJ/mole. The experimental oxidation results here agree with similar alumina scale studies, especially where both $k_{p,i}$ and G_i were characterized. Temperature-sensitive grain enlargement, equilibrium interface P_{O_2} variation, and grain-boundary diffusivities all affect the Arrhenius behavior of scale growth kinetics.

1.0 Introduction: Alumina Scale Growth

Many high-temperature Ni-, Co-, or Fe-based structural alloys and coatings depend on slow-growing alumina scales for oxidation resistance. Consequently, alumina scale growth has been the subject of intense study over many decades, and many excellent reviews are available that provide both a historical perspective of advances and summarize classic key features (Refs. 1 to 4). Briefly, alumina scales are shown to grow primarily by oxygen inward grain-boundary diffusion, with some contributions from outward aluminum grain-boundary diffusion. The presence of one or more reactive element dopants can affect diffusion, most commonly the reduction of outward aluminum diffusion, although no simple relationships between diffusivity and dopants have yet emerged. In any event, scale grain size is shown to be a critical factor, with most models assuming an inverse dependency between effective diffusion and

average grain diameter. Efforts to elucidate diffusional behavior often include $^{16}O/^{18}O$ two-stage or double oxidation tracer studies with nuclear reaction analysis (NRA) or secondary ion mass spectroscopy (SIMS) reconstruction of diffusion profiles. Others utilize growth rate or electrical conductivity variations with P_{O_2}, then model the ionic transport contributions as a function of the P_{O_2} gradient (Refs. 5 to 11). This latter group provided the relations necessary for describing scale growth according to the Wagner relation in which diffusivity is characterized as a function of the chemical potential gradient across the scale. Others address the P_{O_2} gradient in the integration limits for the modified Wagner equation in which $\Delta \ln P_{O_2}$ becomes the salient factor (Refs. 2 and 12 to 15), and many of these will be highlighted later.

The present study is not a critical review or synthesis of the various kinetic studies. Rather, it applies grain-boundary diffusivity relations recently obtained via permeability measurements to the case of scale growth. In those studies diffusion in bulk alumina samples had been elegantly determined through oxygen permeability measurements as a function of P_{O_2} gradients (Refs. 16 to 19). An oxygen flux had been produced across a thin polycrystal of alumina by establishing a P_{O_2} gradient using gas tight seals and controlled 0.01 to 10 vol% O_2/Ar or 0.01 to 1.0 vol% H_2/Ar atmospheres. Typically, a high-P_{O_2} regime was studied by keeping one side of the membrane at 1 Pa O_2 and varying the other to 10^5 Pa. Alternatively, a low-P_{O_2} regime was explored by keeping one side of the membrane at 1 Pa O_2 and varying the other down to 10^{-9} Pa. In some cases the entire pressure regime was studied as a closer simulation to a growing scale. Experiments were performed over the 1500 to 1700 °C temperature range, and O_2 pressure was monitored via zirconia electrochemical cells. Oxygen permeability was determined from the change in steady-state P_{O_2} on one side as the P_{O_2} was changed on the other. The measured permeability and flux were converted to oxygen and aluminum diffusivities at the low- and high-P_{O_2} regimes, respectively, as they followed the expected $P_{O_2}^{-1/6}$ and $P_{O_2}^{+3/16}$ dependencies for n-type oxygen vacancy V_O and p-type aluminum vacancy V_{Al} defect equilibria.

Experimentally, the present study draws from early grain size measurements made for alumina scales formed on a commercial FeCrAl(Zr) alloy, Hoskins 875 (Hoskins Manufacturing Co.), originally intended to verify grain size effects on oxidation rates in early transmission electron microscopy (TEM) studies of NiCrAl scales (Refs. 20 and 21). However, the primary purpose at present is to reconcile alumina growth kinetics and grain-boundary diffusivity obtained by combining the permeability equations with the Wagner model. To accomplish this, a number of relations must be derived. In Section 2.0 we present the basic grain-boundary diffusion equations resulting from the permeability studies. Their incorporation into the Wagner integral, using the concept of effective diffusivity D_{eff} and grain size, yields the general interrelation of the parabolic growth rate constant k_p and oxygen grain-boundary diffusivity at the interface $\delta D_{gb,O,int}$. In Section 3.0, the experimental data set of k_p and grain size are compared with values predicted from $\delta D_{gb,O,int}$. Since the latter is dependent on the P_{O_2} at the metal-scale interface, the thermodynamic calculation of $P_{O_2,eq}$ is first presented. The concept of a constant oxidation product, Π, is then introduced and used to extract $\delta D_{gb,O,int}$ from experimental values of k_p and grain size. Comparable values and activation energies from the literature are noted throughout. Finally, grain-boundary diffusivities obtained from permeability, oxidation, and ^{18}O tracer studies of scales and bulk alumina are compared and discussed.

A list of symbols used in this report is given in Appendix A to aid the reader.

2.0 Development of Diffusivity and Oxidation Equations

This section addresses new relations for Al and O grain boundary diffusivity as obtained from oxygen permeability studies. These are then combined with the standard Wagner analyses that relates scale growth rates to diffusivities.

2.1 Permeability and Grain-Boundary Diffusivity

The assumption of the primary ionic species is essential to the treatment of diffusion across a P_{O_2} gradient in alumina. For the sake of brevity, we consider charged O and Al vacancies ($\left[V_O^{\bullet\bullet}\right]$ and $\left[V_{Al}'''\right]$, respectively) as likely candidates to be formed at interfaces and incorporated as charged polarons diffusing within grain boundaries (Ref. 22). The standard relations connecting defect concentrations with P_{O_2} are developed in Appendix B. These relate the reaction of Al and O to form Al_2O_3 and the formation of charged $\left[V_O^{\bullet\bullet}\right]$ and $\left[V_{Al}'''\right]$ in accordance with equilibrium thermodynamics using Kröger-Vink notation (Ref. 23). Then, electroneutrality is defined for the primary charged ionic vacancies and electron or hole charge carriers. By combining the latter with the equilibrium constants and solving for defect concentrations, one obtains $\left[V_O^{\bullet\bullet}\right]$ proportional to $P_{O_2}^{-1/6}$ at the low-P_{O_2} surface (n-type) and $\left[V_{Al}'''\right]$ proportional to $P_{O_2}^{+3/16}$ at the high-P_{O_2} surface (p-type). Indeed, the grain-boundary diffusivities calculated from permeability studies accordingly yield expected $P_{O_2}^{-1/6}$ (Eq. (1)) and $P_{O_2}^{+3/16}$ (Eq. (2)) dependencies at low (<1 Pa) and high (>1 Pa) P_{O_2}, for oxygen and aluminum vacancies, respectively (Ref. 24). Fe, Ni, Y, Hf, and Zr dopant effects as well as Schottky and Frenkel defect equilibria are significant considerations and have been considered in numerous permeability, conductivity, and oxidation studies. However, the present discussion will refer to the simple $P_{O_2}^{-1/6}$ and $P_{O_2}^{+3/16}$ relations in Appendix B, since they agree with the permeablility results for grain-boundary diffusion in pure alumina. Resulting from this are highly useful relations for both O and Al grain-boundary diffusion (Eqs. (1) and (2), respectively) as a function of temperature and oxygen pressure. From Reference 24,

$$\delta D_{gb,O} = 2.207\times10^{-9}\exp\left(\frac{-467\ \text{kJ}}{RT}\right)P_{O_2,I}^{-1/6}\ \frac{\text{m}^3}{\text{s}\cdot\text{Pa}^{-1/6}} \tag{1}$$

$$\delta D_{gb,Al} = 2.475\times10^{-5}\exp\left(\frac{-604\ \text{kJ}}{RT}\right)P_{O_2,II}^{+3/16}\ \frac{\text{m}^3}{\text{s}\cdot\text{Pa}^{+3/16}} \tag{2}$$

where R is the ideal gas constant, T is temperature, I refers to the low-P_{O_2} surface, and II refers to the high-P_{O_2} surface. These relations therefore define $\delta D_{gb,O}$ and $\delta D_{gb,Al}$ as a function of temperature and oxygen pressure, allowing full predictions of transport across a P_{O_2} gradient, such as in a growing alumina scale. These authors (Ref. 24) applied such equations to FeCrAl oxidation literature values and provided a basis for the extended comparisons developed in this paper. Combined with the appropriate chemical potential gradients, these diffusivities present a strong case in support of primary inward oxygen flux and secondary aluminum outward flux for alumina scale growth (Ref. 24).

As the following sections rely on a number of derivations from various kinetic relations, it may be useful to refer to the flow diagram in Figure 1 for an overall perspective of corresponding sections.

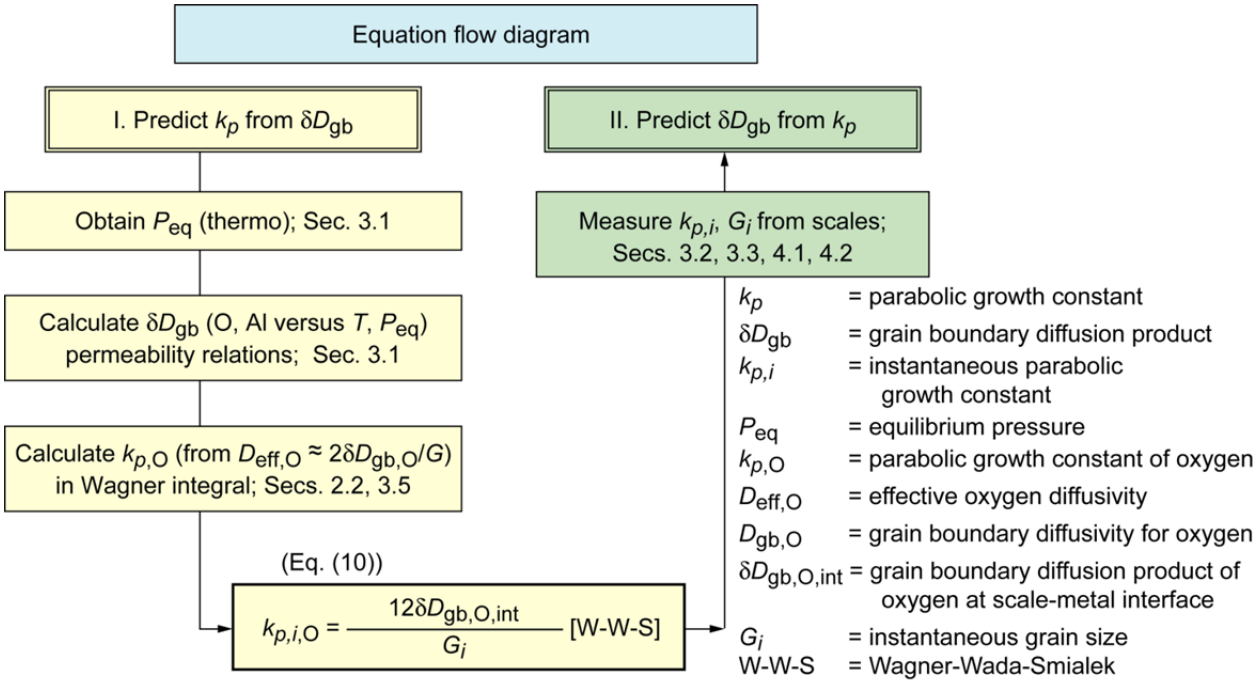

Figure 1.—Derivation scheme relating oxidation to diffusion, then comparative analyses of predicted and measured oxygen diffusivities.

2.2 Oxidation Models

Oxidation processes are generally described by the Wagner relation for the counterdiffusion of ionic species across the chemical potential gradient in the scale, with z_a and z_c ionic charge and D_a and D_c diffusivity of each anion (a) or cation (c) species (Ref. 23). With the parabolic rate constant k_p defined as given below in (Eq. (3)), the appropriate form of the Wagner relation follows as (Eq. (4)). (Note: A factor of 1/2 is often employed before the integral, but corresponds to the less frequently used differential form of $k_p = 1x\cdot dx/dt$, rather than the $k_p = 2x\cdot dx/dt$ definition used here; note t is time. Also, for the purpose of direct comparisons to diffusivities, the thickness form of scaling constants, in m^2/s, was ultimately adopted.)

$$x^2 = k_p t; \quad k_{p,i} = 2x\frac{dx}{dt} \tag{3}$$

$$k_p = \int_{P_{O_2,int}}^{P_{O_2,gas}} \left\{ \frac{z_c}{-z_a} D_c + D_a \right\} d\ln P_{O_2} \tag{4}$$

where z is the valence of anions and cations in the compound. Now, turning to fine grain alumina scales, the importance of grain-boundary diffusion is well recognized and illustrated by the Hart/Smeltzer equations for alumina in Equations (5) and (6) (Refs. 25 to 27). Here the effective diffusion coefficient D_{eff} is a function of the area fraction of short-circuit grain-boundary paths f, often simplified as $2\delta/G$, where δ is the grain-boundary width and G is the grain size (diameter). In the case of alumina, it is generally observed that $D_{gb} >> D_L$ (lattice diffusivity), leading to the following simplification in Equation (6):

$$D_{eff} = (1-f)D_L + fD_{gb} \tag{5}$$

$$D_{\text{eff}} \approx fD_{\text{gb}} = \frac{2\delta D_{gb}}{G} \tag{6}$$

Most transport marker and tracer studies have indicated that the primary growth of alumina scales takes place by oxygen inward diffusion, although some outward growth of alumina scales has been clearly documented (Refs. 28 to 31). For the purpose of illustration, it is assumed here that $D_{\text{gb,O}} >> D_{\text{gb,Al}}$; thus the latter will be omitted from the Wagner integral at present. However, it is also well established that grain "growth" can occur, increasing with scale thickness and temperature. Thus the scale growth rate becomes grain-size dependent and is best treated as an instantaneous value (subscript "*i*"). The resulting expression for $k_{p,i}$ is obtained by substitutions in Equations (3) to (6) to yield

$$k_{p,i} = 2x\frac{\mathrm{d}x}{\mathrm{d}t} = \int_{P_{\text{O}_2,\text{int}}}^{P_{\text{O}_2,\text{gas}}} \frac{2\delta D_{\text{gb,O}}}{G_i}\,\mathrm{d}\ln P_{\text{O}_2} \tag{7}$$

If the diffusion product $\delta D_{\text{gb,O}}$ and grain size are arbitrarily assumed to be invariant across the P_{O_2} gradient, the following oft-used integration for $k_{p,i}$ results:

$$k_{p,i} = \frac{2\delta D^{\times}_{\text{gb,O}}}{G_i}\Delta\ln P_{O_2} \quad [\text{LNP}] \tag{8}$$

Here $\delta D^{\times}_{\text{gb,O}}$ is designated as an approximate or average value and is referred to as the "LNP" solution. However, with the complete P_{O_2} dependence provided by the permeability studies of Wada, Matsudaira, and Kitaoka (Ref. 24), the more precise relations for $k_{p,i}$ are obtained by integrating below, where A is the pre-exponential constant in Equation (10):

$$k_{p,i} = \int_{P_{\text{O}_2,\text{int}}}^{P_{\text{O}_2,\text{gas}}} \frac{2A\exp\left(-Q/RT\right)}{G_i}\left(P_{O_2}\right)^{-7/6}\mathrm{d}P_{O_2} \tag{9}$$

$$k_{p,i} = \frac{2\left(2.207\times10^{-9}\right)\exp\left(-467\ \text{kJ}/RT\right)}{G_i}6\Delta P_{O_2}^{-1/6} \approx \frac{12\delta D_{\text{gb,O,int}}}{G_i} \quad [\text{W-W-S}] \tag{10}$$

Finally, since $\Delta P_{\text{O}_2}^{-1/6} \approx -P_{\text{O}_2,\text{int}}^{-1/6}$, it is seen by inspection that the Wagner integral of the Wada, Matsudaira, and Kitaoka diffusivity $k_{p,i}$ is reduced to a quite simple relation in $\delta D_{\text{gb,O}}$, abbreviated here as the Wagner-Wada-Smialek (W-W-S) solution (Eq. (1)). Furthermore, the deviation in $\delta D_{\text{gb,O}}$ calculated from the W-W-S solution can be shown as an offset from the constant $\delta D^{\times}_{\text{gb,O}}$ (LNP solution, Eq. (8)) by the factor $\Delta\ln P_{\text{O}_2}/6$ in the final relation:

$$k_{p,i} = \frac{12\,\delta D_{\text{gb,O}}}{G_i} \cong \frac{2\,\delta D^{\times}_{\text{gb,O}}\,\Delta\ln P_{O_2}}{G_i} \tag{11}$$

$$\delta D_{\mathrm{gb,O}} \quad [\text{W-W-S}] = \frac{\Delta \ln P_{\mathrm{O_2}}}{6} \delta D^{\times}_{\mathrm{gb,O}} \quad [\text{LNP}] \tag{12}$$

3.0 Experimental and Predicted k_p and $\delta D_{\mathrm{gb,O}}$

Given these derivations and expressions, predictions for k_p (W-W-S) from the Wagner integral will be compared, using these permeability expressions for grain-boundary diffusivity, with those determined experimentally. The results for the reverse calculation, showing what values of $\delta D_{\mathrm{gb,O}}$ are obtained from applying the experimental oxidation results to the W-W-S solution, are then compared to those defined by the permeability expression, Equation (1). Results will also be presented for $\delta D^{\times}_{\mathrm{gb,O}}$, reflecting the departure that occurs if one assumes diffusivity is a constant or average across the $P_{\mathrm{O_2}}$ gradient in the scale. This begins with the necessary thermodynamic treatment to obtain $P_{\mathrm{O_2,int}}$ for the given alloy versus temperature, allowing the calculation of $\delta D_{\mathrm{gb,O}}$ from the permeability expressions. This is followed by a summary of the experimental oxidation results needed to make these comparisons. The k_p and $\delta D_{\mathrm{gb,O}}$ determined from experimental oxidation and diffusion models can then be compared to those predicted by the permeability relations.

3.1 $P_{\mathrm{O_2}}$ Calculations Versus Temperature

The Wagner integration is performed over the $P_{\mathrm{O_2}}$ limits for the scale, from the equilibrium dissociation pressure at the oxide-metal interface to that of the external gas. The former is obtained from the equilibrium constant of the oxidation reaction and the activity of aluminum in the alloy. The approach follows previous studies that predict $P_{\mathrm{O_2,int,eq}}$ from thermodynamic databases and estimate diffusivity from scale growth kinetics (Refs. 10, 12, 14, 15, and 32). For the present example, using a typical Hoskins 875 heater alloy, approximately Fe-22.5Cr-5.5Al-0.5Si-0.2Zr by weight, Al activities were calculated by using the Pandat thermodynamic software package (CompuTherm LLC, Ref. 33) in conjunction with the Paniron database and equilibrium constants obtained from the FactSage thermodynamic database for chemical reactions (Center for Research in Computational Thermochemistry, Ref. 34). The pertinent relations are given below as Equations (13) and (14). The obtained activities a_{Al}, equilibrium constants K_{eq}, and $P_{\mathrm{O_2,eq}}$ are given as a function of temperature in Table I and Figure 2. Given the high degree of linearity, a relation for the equilibrium pressure is also presented (Eq. (15)), obtained by regression of the data with a correlation coefficient of 1.000. This enabled the corresponding $\Delta P_{\mathrm{O_2}}^{-1/6}$ and $\Delta \ln P_{\mathrm{O_2}}$ to be evaluated, as listed in the table. (These essentially converge to $-P_{\mathrm{O_2,int}}^{-1/6}$ and $-\ln P_{\mathrm{O_2,int}}$, respectively, because of the extremely low values of $P_{\mathrm{O_2,int}}$ compared to $P_{\mathrm{O_2,gas}}$.)

$$2\mathrm{Al} + \tfrac{3}{2}\mathrm{O_2} = \mathrm{Al_2O_3} \tag{13}$$

$$K_{\mathrm{eq}} = \frac{1}{a_{\mathrm{Al}}^2 P_{\mathrm{O_2}}^{3/2}} \tag{14}$$

$$P_{\mathrm{O_2,eq}} = 6.117 \times 10^{15} \exp\left(\frac{-1012\ \mathrm{kJ}}{RT}\right)\ \mathrm{Pa} \tag{15}$$

TABLE I.—TEMPERATURE EFFECTS ON THERMODYNAMIC FACTORS FOR ALUMINA SCALES IN EQUILIBRIUM WITH FeCrAl(Zr)[a,b]

[Oxygen pressure at gas surface $P_{O_2,gas} = 2.027 \times 10^4$ Pa.]

Temperature, T, °C	Aluminum activity, a_{Al}	Equilibrium constant,[a] K_{eq}	Oxygen pressure at metal interface, $P_{O_2,int}$, Pa	$\Delta P_{O_2}^{-1/6}$, $Pa^{-1/6}$	$\Delta \ln P_{O_2}$, Pa
1000	9.760×10^{-04}	1.400×10^{52}	1.778×10^{-26}	19573.36	69.21
1100	1.747×10^{-03}	1.245×10^{47}	1.906×10^{-23}	6118.07	62.23
1200	2.896×10^{-03}	5.409×10^{42}	7.861×10^{-21}	2242.40	56.21
1300	4.509×10^{-03}	8.490×10^{38}	1.497×10^{-18}	934.75	50.96
1400	6.665×10^{-03}	3.822×10^{35}	1.514×10^{-16}	432.97	46.34

[a] $K_{eq} = 1/\left(a_{Al}^2 P_{O_2}^{3/2}\right)$ for $2Al + \frac{3}{2}O_2 = Al_2O_3$.

[b] Wagner integral limits on $P_{O_2,eq}$ fixed by corresponding interfacial aluminum activity and equilibrium constant.

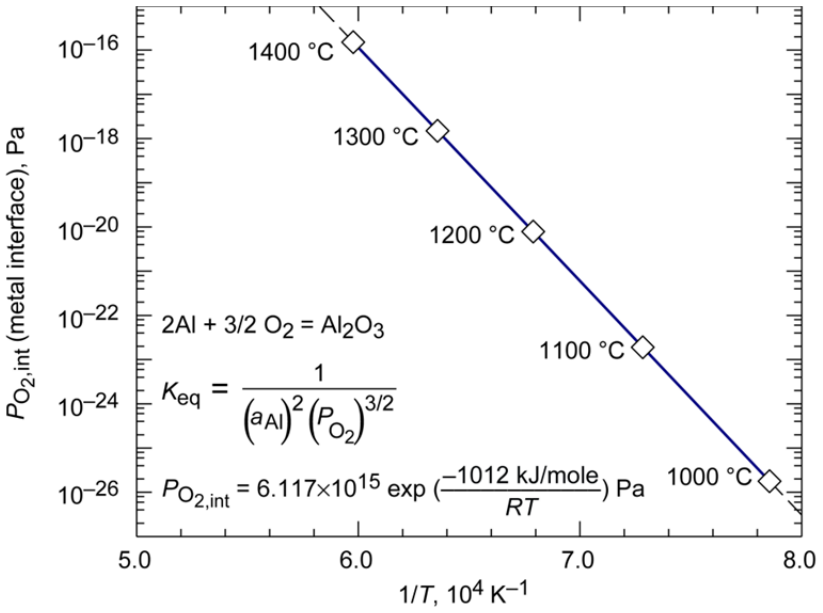

Figure 2.—Equilibrium interfacial $P_{O_2,int}$ calculated from thermodynamics of FeCrAl(Zr)-scale interface using aluminum activity and its reaction with oxygen. Slope of log P versus $1/T$ found to be equivalent to –1012 kJ/mole.

At this point, the relationships between k_p, $\delta D_{gb,O}$ and $P_{O_2,eq}$ can now be employed to evaluate experimental data for scale growth and grain size as a function of time and temperature. However, it is instructive to first illustrate some broad implications for $\delta D_{gb,O}$ and $\delta D_{gb,Al}$ at both sides of the scale and for bulk alumina as well. The gas surface values are obtained from Equations (1) and (2), using $P_{O_2,gas} = 2.027\times10^4$ Pa (0.2 atm). However, the interfacial equilibrium $P_{O_2,int}$ (i.e., referring to the metal-oxide interface) is given by Equation (15). Both result in a modified $A_i' \exp(Q_i'/RT)$ form, where i designates an O or Al ion. $A_{i,gas}'$ is given by $A_i P_{O_2,gas}^n$ and $Q_i' = Q_i$ from Equations (1) and (2). $A_{i,int}'$ is given by $A_i A P_{O_2,gas}^n$ and $Q_{i,int}' = Q_i + n_i Q_{P_{O2}}$, as summarized in Table II (and compared further in Section 5.0).

TABLE II.—GRAIN-BOUNDARY DIFFUSION COEFFICIENTS $\delta D_{gb,X}$ PREDICTED FROM PERMEABILITY RELATIONS[a]

Temperature, T, °C	Grain-boundary diffusivity, m^3/s			
	Oxygen		Aluminum	
	Gas surface (bulk), $\delta D_{gb,gas,O}$	Metal interface, $\delta D_{gb,int,O}$	Gas surface (bulk), $\delta D_{gb,gas,Al}$	Metal interface, $\delta D_{gb,int,Al}$
1000	2.912×10^{-29}	2.976×10^{-24}	2.618×10^{-29}	6.057×10^{-35}
1100	7.241×10^{-28}	2.313×10^{-23}	1.671×10^{-27}	1.431×10^{-32}
1200	1.164×10^{-26}	1.363×10^{-22}	6.066×10^{-26}	1.606×10^{-30}
1300	1.314×10^{-25}	6.416×10^{-22}	1.395×10^{-24}	9.883×10^{-29}
1400	1.111×10^{-24}	2.512×10^{-21}	2.205×10^{-23}	3.712×10^{-27}
Pressure exponent, n	–1/6	–1/6	+3/16	+3/16
Pre-exponential factor, A', m^3/s	4.23×10^{-10}	5.16×10^{-12}	1.59×10^{-04}	2.26×10^{-02}
Activation energy,[a] Q', kJ/mole	467	298	604	794

[a]Pre-exponential factors (A_i') and activation energies (Q_i') are adjusted by pressure, exponents, and energy associated with $P_{O_2,eq}$ in the general Arrhenius form of $\delta D_{gb,i} = A_i' \exp(-Q_i'/RT)$.

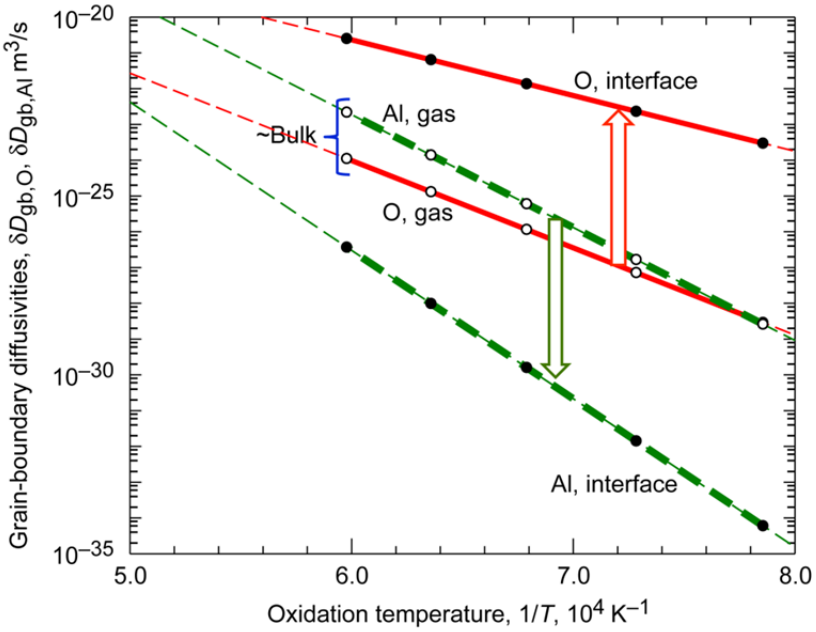

Figure 3.—Grain-boundary diffusivities predicted for alumina scales on FeCrAl(Zr) using permeability relations for aluminum and oxygen at the gas surface and scale-metal interface. Magnitude and slopes change because of large P_{O_2} gradient in scales and temperature-sensitive $P_{O_2,int}^{3/16}$ or $P_{O_2,int}^{-1/6}$ factors.

The limiting relations for δD_{gb} at each reaction surface for each ion are plotted in Figure 3. The highest δD_{gb} is predicted for oxygen at the scale-metal interface, consistent with primary inward growth of alumina scales, as confirmed by virtually every diffusion study for α-Al_2O_3 scales. Oxygen diffusivity at the interface is about 4 to 5 orders of magnitude higher than at the gas surface. Conversely, the highest δD_{gb} for Al occurs at the outer gas surface. It is 3 to 5 orders of magnitude higher than at the scale-metal interface and similar to or slightly above the corresponding $\delta D_{gb,O,gas}$.

The broad arrows in Figure 3 indicate the changes in diffusivity obtained as the scale is traversed inward. The transition between predominantly Al outward to predominantly O inward has been predicted by Wada, Matsudaira, and Kitaoka (Ref. 24) and Matsudaira et al. (Ref. 18) to be extremely close to the gas surface, at just 0.01 percent of the thickness, consistent with the frequent observation of some slight outward growth of alumina scales. Thus they project that double oxidation experiment utilizing $^{16}O/^{18}O$ diffusion profiles actually "probe" levels deeper than this transition and reflect transport still dominated by $\delta D_{gb,O}$.

Finally, it should be pointed out that $\delta D_{gb,O}$ measured on bulk alumina with no P_{O_2} gradient (i.e., self-diffusion) should follow the relations for $\delta D_{gb,O,gas}$, as appropriate to the external pressure. This is suggested as "bulk" behavior in Figure 3 and would be quite lower than (chemical) diffusivity throughout the scale (arrows).

3.2 Oxidation Procedures

To provide comparisons between permeability predictions for scales and actual data, we draw from an older dataset, originally intended to augment some early scale diffusivity discussions for NiCrAl (Refs. 20 and 21). For this purpose, a commercial ferritic FeCrAl(Zr) heater alloy, Hoskins 875, was utilized. The composition is listed in Table III. The alloy was obtained as rolled strip ~1 mm (~40 mil) thick and sectioned into 1.25- by 2.54-cm (0.5- by 1-in.) coupons. These were metallographically polished on emery paper down to a 600-grit finish, washed in detergent, and rinsed ultrasonically in ethanol. Samples were oxidized in high purity alumina boats at 1100, 1200, 1300, and 1400 °C in static ambient air. Weight change was measured for samples pulled at various times up to 1000 h (at 1100 and 1200 °C), 500 h (at 1300 °C), and 100 h (at 1400 °C). (Longer tests at the higher temperatures resulted in chemical failure of the scale at temperature.) Thus, each weight for each time and temperature exposure corresponds to a specific sample. As a consequence, these results may be subject to sample-to-sample variations, especially regarding dx/dt. In a few cases minor spalling was measured in the small crucibles containing the samples and was incorporated into the total mass gain, but it made little difference.

Samples were pulled for grain-size measurements after oxidation for 0.1, 1, 10, 50, 100, 200, 500, and 1000 h, where applicable. Grain size was measured at the oxide-metal interface by detaching the scale. To accomplish this, aluminum stubs were attached to the scale with epoxy, then detached by pulling in a tensile adhesion test jig. Numerous representative micrographs of the underside of the alumina grains were obtained by SEM. Also, the corresponding grain imprints in the exposed metal side of the coupon were measured. The recorded grain size was the largest diameter of a grain, averaged over ~100 grains measured for a given test condition.

The underside of representative scale samples are presented in Figure 4. Figure 4(a) shows the noticeable temperature effect on the enlargement of grains formed after 100 h, and Figure 4(b) shows the time effect for grains formed at 1400 °C. At higher temperatures, a tendency for dimpled grains was noticed. These were matched and in contact with intergranular protrusions on the metal side and so were not voids. These features may indicate an increasing inward oxygen flux in the vicinity of the grain-boundary relative to that along the lateral interface at higher temperatures.

TABLE III.—COMPOSITION (wt.%) OF FeCrAl(X) ALLOYS WHERE OXYGEN GRAIN-BOUNDARY DIFFUSIVITY $\delta D_{gb,O}$ IS PREDICTED FROM OXIDATION KINETICS AND GRAIN SIZE

Study	Alloy	Alloy composition, wt%						
		Fe	Cr	Al	Si	Zr	Y	Other
Smialek (current study)	Hoskins 875	Bal.	22.5	5.5	0.5	0.2	----	----
Naumenko (Ref. 35)	FeCrAlY	Bal.	19.9	5.00	0	----	0.051	----
Messaoudi (Ref. 36)	Imphy	Bal.	22.6	4.36	0.85	0.13	----	0.38 Mn, 0.35 Ni
Ramanarayanan (Ref. 10)	MA956	Bal.	20.0	4.5	----	----	----	0.5 Ti, 0.5 Y_2O_3

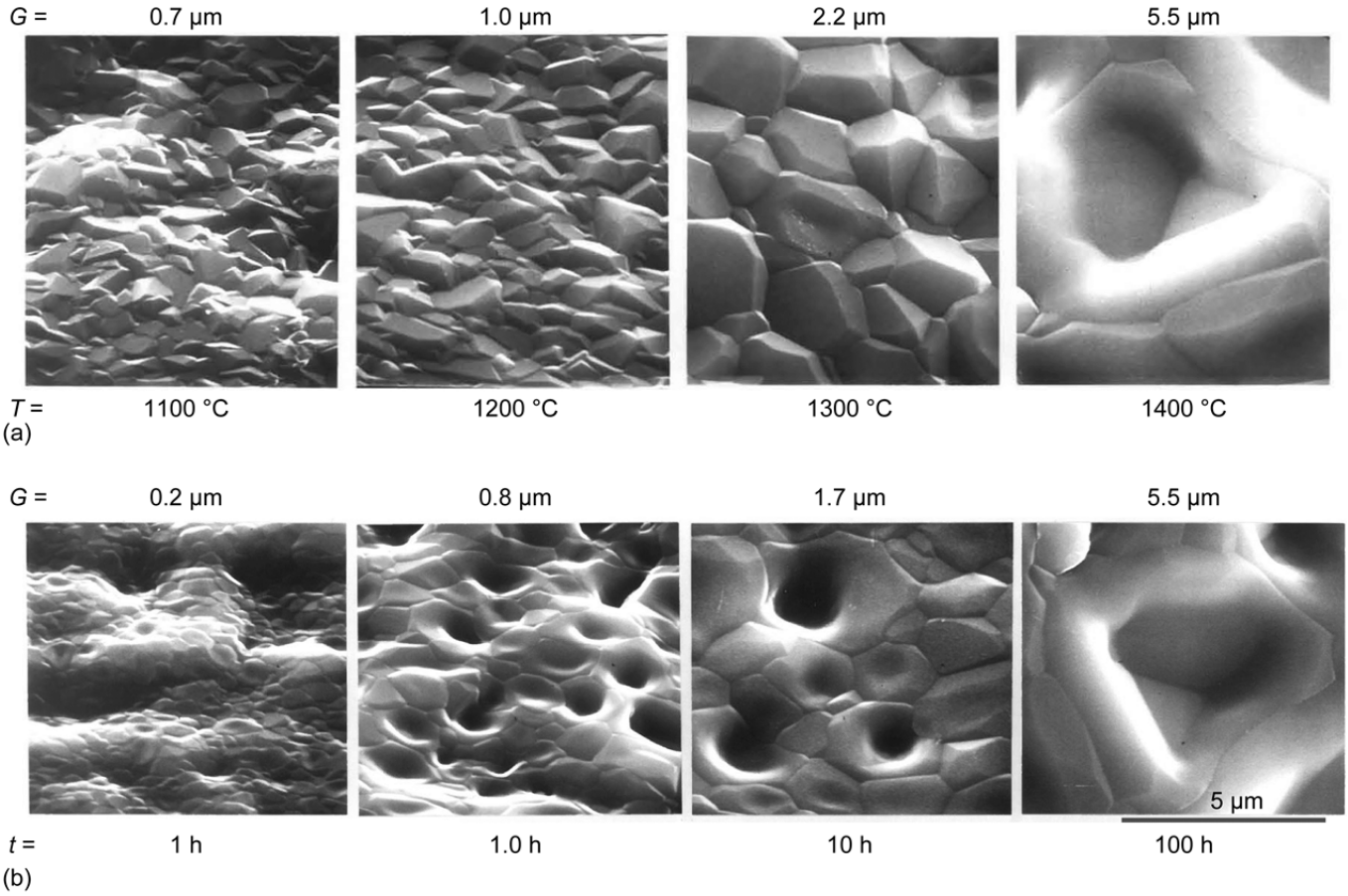

Figure 4.—Representative scale (underside) structures stripped from oxidized FeCrAl(Zr) alloy, showing alumina grain size *G* increases from 0.2 to 6 μm (on average). (a) Oxidation at 100 h for different temperatures *T*. (b) Oxidation at 1400 °C for different times *t*.

3.3 Experimental Weight Gain and Grain Size Data

The weight gain and interfacial grain size data are given in Table IV. Although the details of the kinetic behavior are the subject of another study, it is noted that the weight gain was subparabolic, yielding a time exponent of $t^{0.37}$, while grain size followed a $\sim t^{0.26}$ dependence, on average. This is quite consistent with D_{eff} being inversely related to grain size, where a $t^{0.375}$ oxidation law was predicted for the $t^{0.25}$ grain "growth." (Oxidation time exponents ($1/n$) and grain growth time exponents ($1/m$) are related by $n = 2m/(m–1)$, Refs. 21, 37, and 38). The $t^{0.37}$ rate is similar to the cubic FeCrAl(Y) oxidation law presented by Quadakkers et al. (Refs. 38 and 39).

Similary, the grain expansion can be assessed in relation to the findings of Naumenko et al. for the case of FeCrAlY oxidized at 1200 and 1250 °C (Ref. 35). Here grain size *G*, elegantly measured by EBSD (electron backscatter diffraction) of FIB (focused ion beam) cross sections, was found to be a temperature-invariant function of scale thickness *x* in the form $G = 0.27 + 0.13x$ (both in μm). Using weight gain obtained in the present study of FeCrAl(Zr) (converted to 5.34 μm thickness for each mg/cm^2 of oxygen gained) from Table IV, interfacial grain size versus scale thickness was plotted in Figure 5. It is seen that the thinner scales cluster along the single curve of the Naumenko relation; however, positive deviation appears significant at the higher 1300 and 1400 °C temperatures. In any event, the importance of increasing grain size for thicker scales is clearly demonstrated. This treatment simply employs the instantaneous grain size (Table IV).

TABLE IV.—PERTINENT SCALE GROWTH AND GRAIN SIZE DATA USED TO ESTIMATE Π_i AND $\delta D_{gb,O}$ FOR HOSKINS 875[a]

(a) 1100 °C

Time, h	Scale weigh gain, x, mg/cm^2	Scale growth rate, dx/dt mg/cm^2·h	Grain size, G, μm	Oxidation product,[a] Π, μm^3/h
0.1	-----	-----	-----	-----
1	0.027	-----	0.56	-----
10	0.192	1.02×10^{-02}	0.42	4.69×10^{-02}
50	0.438	4.25×10^{-03}	0.59	6.28×10^{-02}
100	0.591	2.24×10^{-03}	0.70	5.28×10^{-02}
200	0.752	1.36×10^{-03}	0.62	3.61×10^{-02}
500	1.010	3.92×10^{-04}	1.01	2.28×10^{-02}
1000	1.077	4.80×10^{-05}	1.18	3.48×10^{-03}

(b) 1200 °C

0.1	-----	-----	-----	-----
1	0.152	-----	-----	-----
10	0.453	1.66×10^{-02}	0.53	2.27×10^{-01}
50	0.731	6.67×10^{-03}	0.80	2.22×10^{-01}
100	1.153	3.94×10^{-03}	1.05	2.72×10^{-01}
200	1.38	2.10×10^{-03}	1.07	1.77×10^{-01}
500	1.725	8.00×10^{-04}	2.18	1.72×10^{-01}
1000	1.979	4.19×10^{-04}	1.66	7.85×10^{-02}

(c) 1300 °C

0.1	0.125	9.50×10^{-01}	0.45	3.05
1	0.492	1.87×10^{-01}	0.75	3.93
10	0.910	3.62×10^{-02}	1.25	2.35
50	-----	-----	-----	-----
100	2.147	8.50×10^{-03}	2.22	2.31
200	2.801	5.17×10^{-03}	3.67	3.03
500	3.713	1.20×10^{-03}	4.09	1.04
1000	-----	-----	-----	-----

(d) 1400 °C

0.1	0.246	$1.70\times10^{+00}$	0.58	$1.38\times10^{+01}$
1	0.764	3.43×10^{-01}	1.27	$1.90\times10^{+01}$
10	1.731	7.12×10^{-02}	2.31	$1.62\times10^{+01}$
50	-----	-----	-----	-----
100	4.063	1.13×10^{-02}	5.51	$1.44\times10^{+01}$
200	-----	-----	-----	-----
500	-----	-----	-----	-----
1000	-----	-----	-----	-----

[a]Π_I is oxidation product Π_i (= $k_{p,i}\cdot G_i$, where $k_{p,i}$ is the instantaneous value of the parabolic growth constant and G, the instantaneous grain size) at the low-oxygen-pressure surface. $\delta D_{gb,O}$ is the oxygen grain-boundary diffusion product.

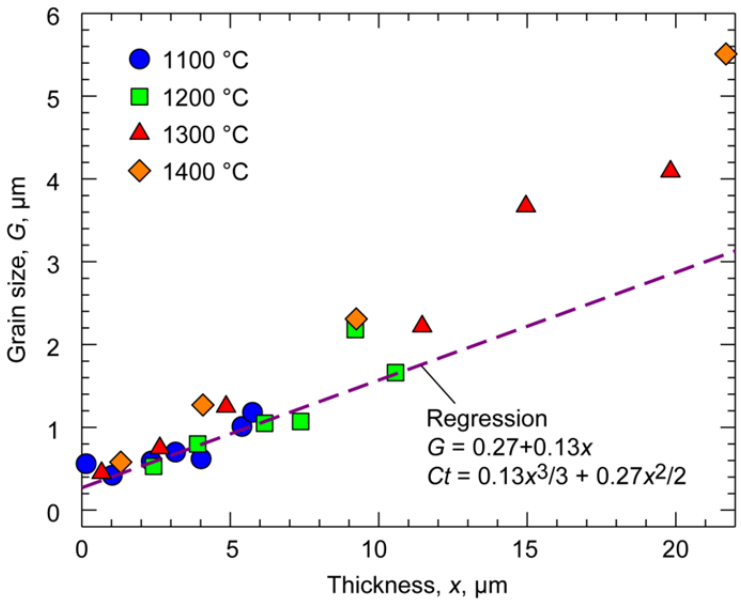

Figure 5.—Correlation of interfacial scale grain size G with scale thickness x estimated from oxidative mass gain from interrupted FeCrAl(Zr) oxidation at 1100 to 1400 °C. Comparison to relation for scale cross sections produced by Naumenko et al. for 1200 and 1250 °C oxidation (Ref. 35). Here C is 0.2273 µm^3/h and t is time (5.34 µm thickness conversion for every 1 mg/cm^2 oxidative mass gain).

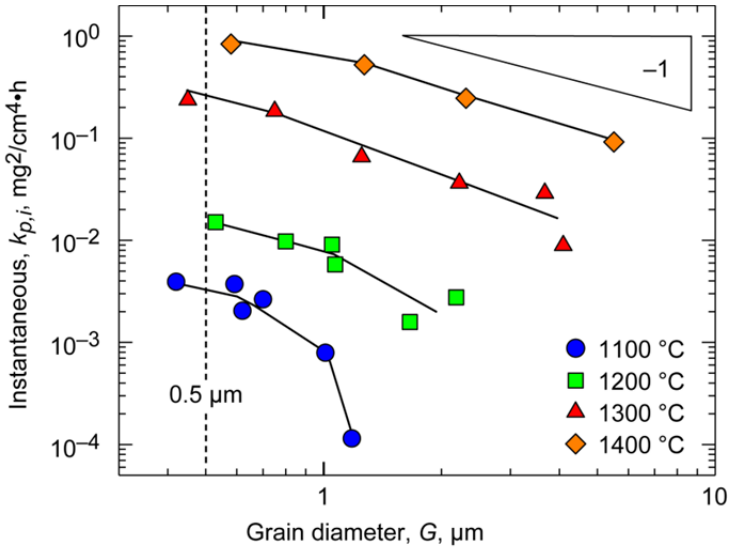

Figure 6.—Relationship of FeCrAl(Zr) instantaneous parabolic oxidation constant $k_{p,i}$ to grain size G. Initial portions (at ~0.5 µm) indicate an inverse G^{-1} relationship holds at all four temperatures (1 mg^2/cm^4•h = 7.918×10^{-15} m^2/s).

The corresponding specific, individually measured, instantaneous $k_{p,i}$ were determined from Equation (3), obtaining dx/dt graphically from the slope of x versus t plots. The variation with grain size is given in Figure 6. The initial values of $k_{p,i}$ decrease at the predicted rate according to G^{-1}. These portions are thus consistent with the treatment of $k_{p,i}$ as a function of $D_{\text{eff}} = 2\delta D_{\text{gb.O}}/G_i$ (Eq. (10)), with $\delta D_{\text{gb.O}}$

assumed to be constant with time. They are therefore considered suitable for assessing grain-boundary diffusion as an invariant parameter in the scaling process. The minor fluctuations in each curve are believed to arise from graphically determining $2x \cdot dx/dt$ from a single oxidation curve generated by multiple samples, with perhaps some sample-to-sample variation, rather than using one continuous curve for one sample. Additionally, the variation in grain size could be substantial within any given sample, but the average values of many measurements should provide valid trends.

3.4 Arrhenius Behavior of $k_{p,i}$

For purposes of consistent comparisons and subsequent calculation of a deconvoluted activation energy, the instantaneous $k_{p,i}$ were determined at the same grain size (0.5 μm) for each temperature. Other grain sizes would also be appropriate for this analysis, up to about 1 μm, according to Figure 6. An Arrhenius plot of the aforementioned $k_{p,i,0.5,}$ is presented in Figure 7. The fitted relation for $k_{p,i,0.5}$, (r^2 correlation coefficient of 0.98) is given by Equation (16) and shows an activation energy of 375 kJ/mole.

$$k_{p,i,\text{exptl}} = 4.29 \times 10^{-3} \exp\left(\frac{-375\,\text{kJ}}{RT}\right) \text{m}^2/\text{s} \tag{16}$$

This curve is now compared with data from the literature, where grain size was provided in addition to kinetics. Both parameters are available unequivocally from the study of Naumenko et al. (Ref. 35). Here, well-defined data were examined to determine the equivalent thickness for a 0.5-μm grain size for scales grown on FeCrAlY (Table III) at 1200 °C. Their equation for grain size yields a scale thickness of 1.77 μm for an interface grain size of 0.5 μm. This was then used in their cubic polynomial describing scale growth, $0.13x^3/3 + 0.27x^2/2 = Ct$, where C can be shown to be 0.2273 μm^3/h. Differentiating and solving for $2x\ dx/dt$ yields $2C/G$. At $G = 0.5$ μm, $2C/G$ yields 0.909 μm^2/h or 2.525×10^{-16} m^2/s for $k_{p,i}$. The latter value, plotted as the square symbol in Figure 7, is seen to fall directly on the 0.5-μm regression curve for the present FeCrAl(Zr) alloy. This agreement provides some degree of confidence with the present technique in which separate samples were used to determine $k_{p,i}$ and G_i.

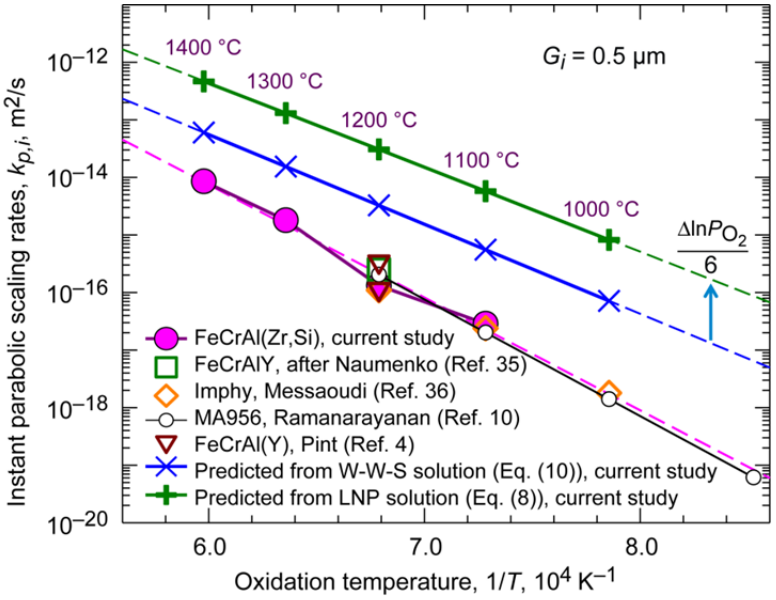

Figure 7.—Instantaneous $k_{p,i}$, measured for G_i = 0.5 μm, compared to predictions from permeability relations. Experimental data at G ≈ 0.5 μm all agree for FeCrAl alloys studied.

Similarly, the oxidation behavior of an Imphy FeCrAl(Zr,Si) alloy (Imphy Alloys, Inc.) (see Table III) by Messaoudi, Huntz, and Lesage (Ref. 36) is presented as open diamonds. Here the 48-h average parabolic growth rate $k_{p,\mathrm{avg}}$ was reported, but it corresponds to similar but slightly varying $G_{48\mathrm{h}}$ = 0.3, 0.6, and 0.8 μm at 1000, 1100, and 1200 °C, respectively. Again, the data are seen to fall near the present data or regression line. Finally, the average 100-h data of Ramanarayanan et al. (Ram) from Reference 10 for MA956 (an FeCrAl-Y_2O_3 alloy, Special Metals Corp.), Table III, oxidized at 900 to 1200 °C, are presented according their Arrhenius relation, converted to kilojoules and meters squared per second:

$$k_{p,i,100}\,[\mathrm{Ram}] = 1.20\times10^{-2}\exp\left(\frac{-388\,\mathrm{kJ}}{RT}\right)\ \mathrm{m}^2/\mathrm{s} \tag{17}$$

Here it should be noted that a relatively constant grain size of 0.5 μm was reported for the 100-h TGA (thermogravimetric analysis) test (increasing to only 0.75 and 1.25 μm for 300- and 1000-h exposures, respectively). This effectively allows direct comparison with the present $k_{p,i}$ data and is seen to lie essentially on the same line.

3.5 $k_{p,i}$ Predicted From W-W-S Permeability Relations

Having established a valid Arrhenius plot of $k_{p,i}$ (i.e., without grain growth), it is now possible to compare predicted k_p from the permeability studies and the W-W-S solution (Eq. (10)) developed above, all for a grain size of 0.5 μm. Using the permeability equation reported for $\delta D_{\mathrm{gb,O}}$ and the values for $\Delta P_{\mathrm{O}_2}^{-1/6}$ from Table I, the values shown as "×" in Figure 7 are produced. These are higher than those determined from oxidation experiments and result in an activation energy of 298 kJ/mole, somewhat below the 375 kJ/mole determined from oxidation. The Arrhenius dependency obtained with r^2 = 1.000, when combining equations for $\delta D_{\mathrm{gb,O}}$ and $P_{\mathrm{O}_2,\mathrm{int}}$ in the W-W-S solution (Eqs. (1), (10), and (15)), is given by

$$k_{p,i}\,[\mathrm{W\text{-}W\text{-}S}] = 1.24\times10^{-4}\exp\left(\frac{298\,\mathrm{kJ}}{RT}\right)\ \mathrm{m}^2/\mathrm{s} \tag{18}$$

As will be discussed later, the discrepancy between the refined oxidation data (Eq. (16)) and the derived W-W-S solution (Eq. (18)) may be due in large part to the fact that the former pertains to doped alumina scales while the latter pertains to pure alumina.

3.6 $k_{p,i}$ Prediction Assuming P_{O_2}-Independent Diffusivity (LNP Integral)

As will be discussed below, analyses of alumina scale growth frequently assume a constant diffusivity across the scale. The permeability studies of Matsudaira (Ref. 18) suggest that this is somewhat true for much of the thickness for the proposed oxidation case modeled for FeCrAlY (Y_2O_3) alloys at 1100 °C and an interfacial P_{O_2} of ~10^{-23} Pa. Their model predicts δD_{gb} across the much of scale is close to that given by the P_{O_2} at the interface (10^{-23} Pa). A simple comparison of the LNP solution to the W-W-S solution was given as Equation (12) and can be shown to be approximately a factor of 8 to 11 higher:

$$\frac{k_p\,[\mathrm{LNP}]}{k_p\,[\mathrm{W\text{-}W\text{-}S}]} = \frac{\Delta \ln P_{\mathrm{O}_2}}{6} \approx \frac{\ln P_{\mathrm{O}_2,\mathrm{int}}}{6} \approx 10 \tag{12b}$$

This is presented as the topmost LNP curve in Figure 7 and is seen to have a slightly lower activation energy and to deviate further from the experimental data. Alternatively, experimental values of $k_{p,i}$ can be used to predict the grain-boundary diffusion product $\delta D_{gb,O,int}$ by both the W-W-S or LNP approaches, then compared to those predicted by permeability studies from Equation (1) as well as values obtained from tracer studies on bulk alumina. These results are presented in the following section.

4.0 $\delta D_{gb,O}$ Predicted From Permeability Relations and Oxidation Data

The permeability studies have offered relations allowing for the prediction of $\delta D_{gb,O}$ once the $P_{O_2,int}$ has been determined. This enabled the prediction of oxidation rates for given scale grain sizes using both the LNP and W-W-S solutions to the Wagner equation (Eqs. (8) and (10)) and comparison to those actually measured. In the following the reverse occurs; namely, estimates of $\delta D_{gb,O}$ are obtained from the oxidation data and then compared to those predicted by the permeability and ^{18}O tracer studies of bulk alumina.

4.1 Time-Invariant Oxidation Product, Π

In order to properly assess the calculation of $\delta D_{gb,O,int}$ from oxidation data, it is first useful to introduce the concept of a time-invariant constant scaling product, $\Pi_i = k_{p,i} \cdot G_i$. This follows from Equation (10) when the inputs to the Wagner integral, the diffusion product δD_{gb} and P_{O_2} at the interface (fixed by interface composition), do not change with time. Accordingly, the experimental values of Π_i are presented as a function of time for the four temperatures of this study in Figure 8. (The use of $t^{1/2}$ as the x-axis is of no mechanistic significance; it was adopted merely to provide a reasonable comparison of the data without going to the extreme of a log scale). The plot does suggest invariance of Π_i, at least for most of the initial portion of the oxidation curves. The dashed lines indicate average values for the invariant regions (first three or four data points to about 200 h). An appreciable drop in Π_i is noted at long 500- to 1000-h exposures and suggests a reduction in δD_{gb} or an increase in $P_{O_2,int}$, perhaps due to aluminum depletion.

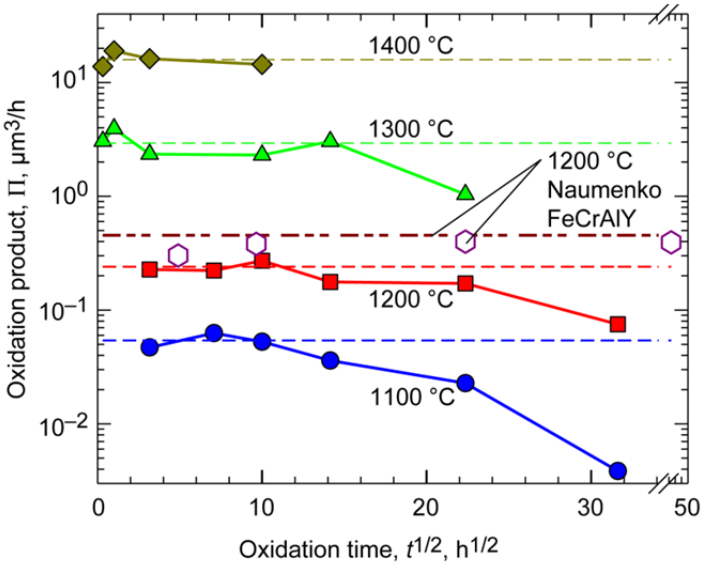

Figure 8.—Invariance of instantaneous oxidation product, Π_i, for FeCrAl(Zr) reflecting growth by constant $\delta D_{gb,O}$. Comparison to invariant 1200 °C values determined for FeCrAlY by Naumenko et al. (Ref. 35).

Finally the rigorously measured 1200 °C FeCrAlY data of Naumenko et al. (Ref. 35) are presented here as open symbols for $k_{p,i} \cdot G_i$. Here grain size data (G) and scale thickness (x) (from Figs. 6 and 10 in Ref. 35) were used for samples oxidized for 24, 93, 500, and 2000 h. The quantity dx/dt was estimated graphically (from curves in Fig. 10 of Ref. 35). Thus $k_{p,i} = 2x\ \mathrm{d}x/\mathrm{d}t$ and $\Pi_i = k_{p,i} \cdot G_i$ were evaluated from the raw experimental data (symbols). It is also noted that Π_i may be obtained more analytically from their relations for $x(t)$ and $G(t)$ determined from the continuous 100-h isothermal oxidation TGA data. It can be shown that $2C = k_{p,i}G_i = \Pi_i$, a constant equal to 0.4546 μm^3/h (1.263×10^{-4} μm^3/s) (dashed line) and implies δD_{gb} for the more general case.

4.2 FeCrAl(Zr) Oxidation Results (This Study)

With well-behaved kinetic behavior established under defined microstructural conditions, experimental $k_{p,i}$ and G_i can now be used to predict δD_{gb} derived from scale growth data. Again the W-W-S solution (Eq. (10)) is employed, but in reverse. The resulting behavior is given in the Arrhenius plot of Figure 9. The same activation energy and correlation coefficient of $r^2 = 0.98$ are obtained, and the full relation given as–

$$\delta D_{gb,O}\ (\text{oxidation}) = 1.79\times10^{-10} \exp\left(\frac{-375\ \text{kJ}}{RT}\right)\ \text{m}^3/\text{s}\ \ [\text{W-W-S}] \tag{19}$$

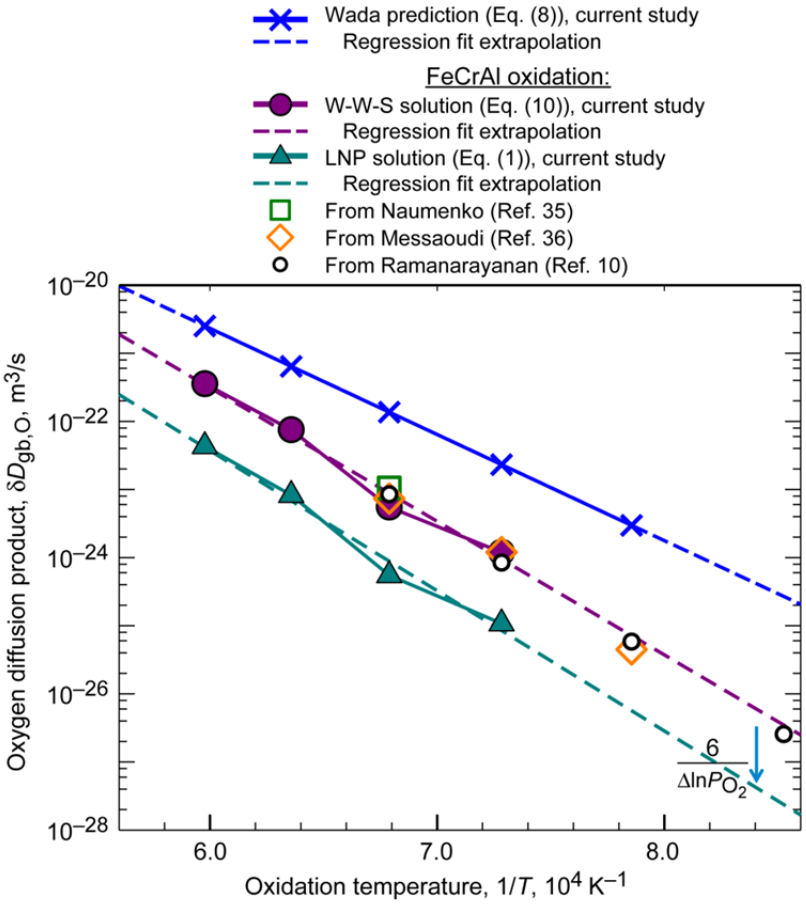

Figure 9.—Oxygen grain-boundary diffusion product $\delta D_{gb,O}$ estimated from FeCrAl(Zr) oxidation and W-W-S solution, Equation (10) of current study. Shows agreement with literature value calculations, but offsets from permeability predictions.

The same offset is seen from the values predicted from permeability relations here as found for $k_{p,i}$ in Figure 7. Values of $\delta D_{\mathrm{gb,O,int.}}$ determined from the Wada, Matsudaira, and Kitaoka (Ref. 24) relations in Equation (1) using the interface values of $P_{\mathrm{O_2,eq}}$ in Table I yield

$$\delta D_{\mathrm{gb,O}}\ (\text{permeability}) = 5.16\times10^{-12}\exp\left(\frac{-298\ \mathrm{kJ}}{RT}\right)\ \mathrm{m^3/s}\ [\text{Wada}, \delta D_{\mathrm{gb}}] \tag{20}$$

Also, $\delta D^{\times}_{\mathrm{gb,O}}$ treated as an average or constant value across the $P_{\mathrm{O_2}}$ gradient (outside the Wagner integral) yields the LNP solution (Eqs. (8) and (11)):

$$\delta D^{\times}_{\mathrm{gb,O}}(\text{oxidation}) = 8.12\times10^{-11}\exp\left(\frac{-394\ \mathrm{kJ}}{RT}\right)\ \mathrm{m^3/s}\ [\text{LNP}] \tag{21}$$

This is seen in Figure 9 (filled triangles) to be below that produced by using the experimental data in the W-W-S solution, again by the factor $\Delta\ln P_{\mathrm{O_2}}/6$ as expected from Equation (12). The differences reflect the $\Delta P_{\mathrm{O_2}}^{-1/6}$ versus $\Delta\ln P_{\mathrm{O_2}}$ integration limits for the two expressions in the Wagner integral.

Also shown are literature values obtained as in Figure 7, when the grain size was known well enough to estimate the oxidation product Π. They are seen to essentially lie on the same curve as the present data.

4.3 Comparisons to Oxidative Literature Values for $\delta D^{\times}_{\mathrm{gb,O}}$

Now Figure 10 compares the $\delta D^{\times}_{\mathrm{gb,O}}$ results for the LNP solution with similar values obtained from the oxidation literature. Data from Young et al. (Ref. 12), obtained from the same FeCrAlY alloy as Naumenko et al. (Ref. 35), are included as the cross-square symbols (Eq. (16) in Ref. 12). They are seen to fall close to values predicted for the present data using this LNP formula (i.e., assuming that $\delta D_{\mathrm{gb,O}}$ is independent of $P_{\mathrm{O_2}}$). Also included are data similarly obtained for Y_2O_3-dispersion-strengthened FeCrAl, MA956 (Refs. 13 and 14), with a reported activation energy of 294 kJ/mole, as compared to the 394 kJ/mole determined from the LNP analyses of the present FeCrAl(Zr) data. The same alloy had been characterized earlier by Ramanarayanan et al. (Ref. 10). Using their reported average k_p and grain size, the LNP results are again seen to fall exactly on the line representing the present study, with an activation energy of 388 kJ/mole, and remarkably close to those reported by Clemens et al. for this alloy (Ref. 14). However, Ramanarayanan et al. (Ref. 10) also performed their own $\delta D_{\mathrm{gb,O}}$ analyses but arrived at a different expression:

$$\delta D^{\times}_{\mathrm{gb,O}}(\text{oxidation}) = 4.92\times10^{-8}\exp\left(\frac{-560\ \mathrm{kJ}}{RT}\right)\ \mathrm{m^3/s} \tag{22}$$

This was seen to diverge to substantially higher values of $\delta D_{\mathrm{gb,O}}$ and is not shown here. It is also said to be adjusted by $P_{\mathrm{O_2}}^{-1/6}$, presumably for the environmental test atmosphere, the gas surface.

Furthermore, an analogous LNP analysis was performed on the MAX compound, Ti_3AlC_2 (Ref. 32), shown as the crossed diamonds in Figure 10. Except for short times, especially at lower temperatures, the scales were primarily α-Al_2O_3. Their results are very close to that presented for the four FeCrAl alloys in Figure 10, and linear regression produced 375 kJ/mole. In total, the plot in Figure 10 shows reasonable agreement from seven separate studies. Although this agreement in experimental data is encouraging, it does not necessarily indicate that the LNP solution is the preferred method of calculating $\delta D_{\mathrm{gb,O}}$. It just means that there are many studies with an available $\delta D^{\times}_{\mathrm{gb,O}}$ determined this way. Had all the studies provided $k_{p,i}$ and corresponding G_i data one could evaluate the same studies via the W-W-S solution as well.

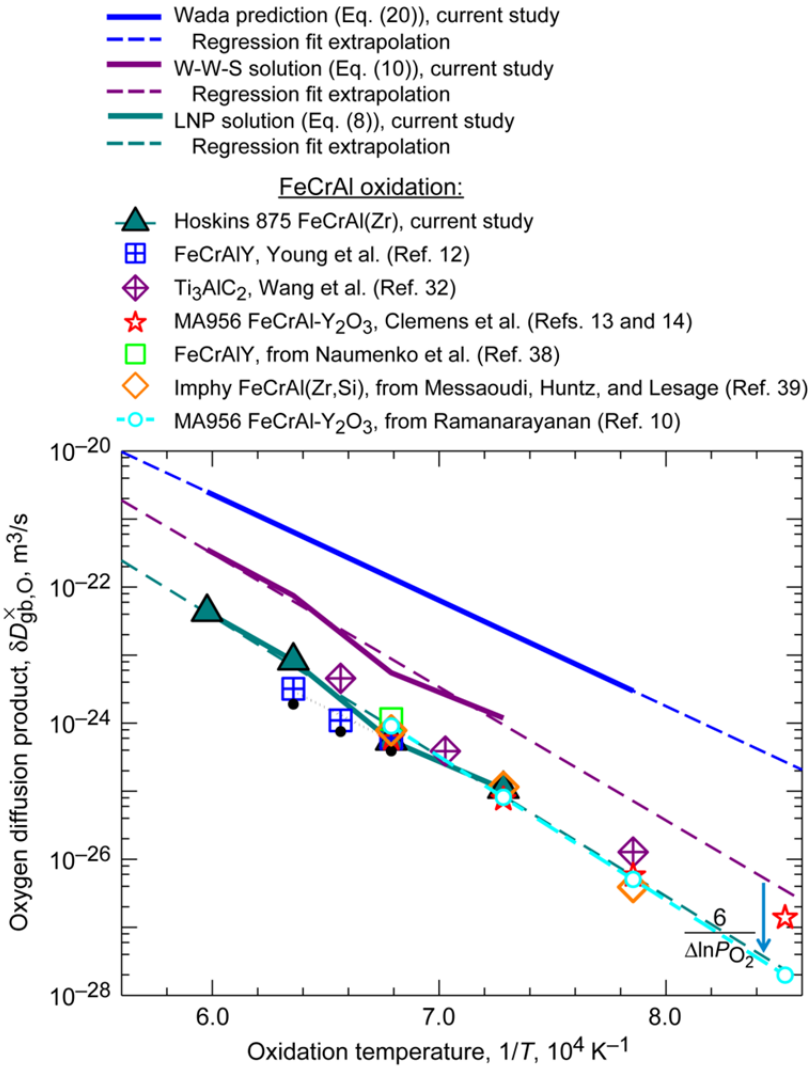

Figure 10.—Average oxygen grain-boundary diffusion product $\delta D^{\times}_{gb,O}$ for FeCrAl(X) alloys. Literature values from Young (Ref. 12), Wang (Ref. 32), and Clemens (Ref. 14) agree with those obtained here by LNP solution for alumina scale growth.

Regarding the two W-W-S and LNP techniques used to calculate $k_{p,i}$ from $\delta D_{gb,O}$, it is again useful to recall the standard factor relating these terms as stated in Equations (8) and (10). Here it was shown that the factor relating $k_{p,i}$ (LNP), as a constant or average $\delta D^{\times}_{gb,O}$, to the $k_{p,i}$ (W-W-S) was $\Delta \ln P_{O_2} / 6$ (Eqs. (11) and (12)). This offset was indicated in Figure 7. Conversely, any $\delta D_{gb,O}$ determined from the same experimental $k_{p,i}$ using a constant $\delta D^{\times}_{gb,O}$ outside the Wagner integral will be the inverse factor of $6/\Delta \ln P_{O_2}$ times $\delta D_{gb,O,int}$ determined from the W-W-S relation. This factor is so indicated in Figures 9 and 10. It is thus seen that the LNP analyses predicted k_p further from the experimental k_p (Fig. 7) or $\delta D_{gb,O,int}$ further from the permeability derived relations than did the W-W-S analyses (Fig. 9).

4.4 Comparison With $\delta D_{gb,O}$ Measured by ^{18}O Tracer Studies

Finally, as with most discussions of diffusion in alumina scales, a more global perspective is provided by comparing these predictions with summary plots of diffusion in alumina, such as those recently discussed by Heuer et al. (Refs. 22 and 40) in Figure 11. Here $\delta D_{gb,O}$ data measured from ^{18}O tracer experiments for both bulk alumina (under no P_{O_2} gradient) and alumina scales (growing in a large gradient) are compared. The top curve (i) is that obtained by applying the Wada, Matsudaira, and Kitaoka (Ref. 24) relation for diffusivity to the low P_{O_2} interface on a growing scale (Eqs. (1) and (20), Table II). The middle curve (ii) is that predicted from the present data for alumina scales formed on Hoskins 875 FeCrAl(Zr) (Eqs. (10) and (18)). Here oxidation kinetic and grain size data use the W-W-S solution, predicting diffusivity from Π_i ($k_{p,i}$ and G_i). The next curve (iii) is that obtained from the same oxidation data, but now using the $\Delta \ln P_{O_2}$ solution (LNP, assuming a constant average $\delta D^{\times}_{gb,O}$, Eqs. (8), (11), and (21)). The individual data points for curves 1 to 3 had been shown in Figures 9 and 10. The lowest curve (iv) was obtained from the permeability-derived equation for $\delta D_{gb,O,gas}$ for the case of exposure to 1 atm air, with no P_{O_2} gradient (Eq. (1), Table II, Fig. 3).

The ^{18}O tracer studies for bulk alumina refer to pure or Mg-doped Al_2O_3 for Reddy and pure or Y-doped Al_2O_3 from Prot et al. (Refs. 41 to 43). Only curve 4, appropriate for bulk alumina without a P_{O_2} gradient, appears to approach magnitudes of the undoped or Mg-doped Al_2O_3, but the data are quite high compared to that extrapolated from Y-doped Al_2O_3. Curve 4 does not have an activation energy similar to any of these, but at least is much closer than any predictions for $\delta D_{gb,O}$ appropriate for oxidation (curves 1 to 3).

The ^{18}O tracer studies for double oxidation of FeCrAl alloys refer to those of Messaoudi et al. (circles, squares, and diamonds) (Ref. 36) and Chevalier et al. (triangles) (Ref. 44). The 1100 °C point for MA956 (Refs. 14 and 45) is also included (dotted hexagon) as it corresponds to fitting an ^{18}O SIMS profile. All the alloys of Messaoudi are in the vicinity of curve (iv) for bulk alumina, whereas the undoped alloy of Chevalier (open triangles) is grouped near curve (ii) predicted for growing scales. The Y-doped alloy (filled triangle), however, is near the Messaoudi data and curve (iv). The Clemens/ Bongartz point falls directly on the permeability LNP solution, as in Figure 10. Thus only some ^{18}O tracer data seems comparable to the appropriate permeability predictions. These inconsistencies are difficult to resolve and underscore the challenges encountered with measuring or predicting diffusivity in alumina scales and comparing the same to that measured for bulk alumina. (It should be noted that more measurements for bulk alumina from Reference 44 (not shown) fall between the oxidation values, far from other bulk data, and are not reconciled here). Overall it is seen, as in Figure 3, that the P_{O_2} gradient in a scale can result in diffusivities expected to be 3 to 5 orders of magnitude greater than for bulk alumina in no P_{O_2} gradient. It also appears that some double oxidation experiments may reflect this in varying degrees.

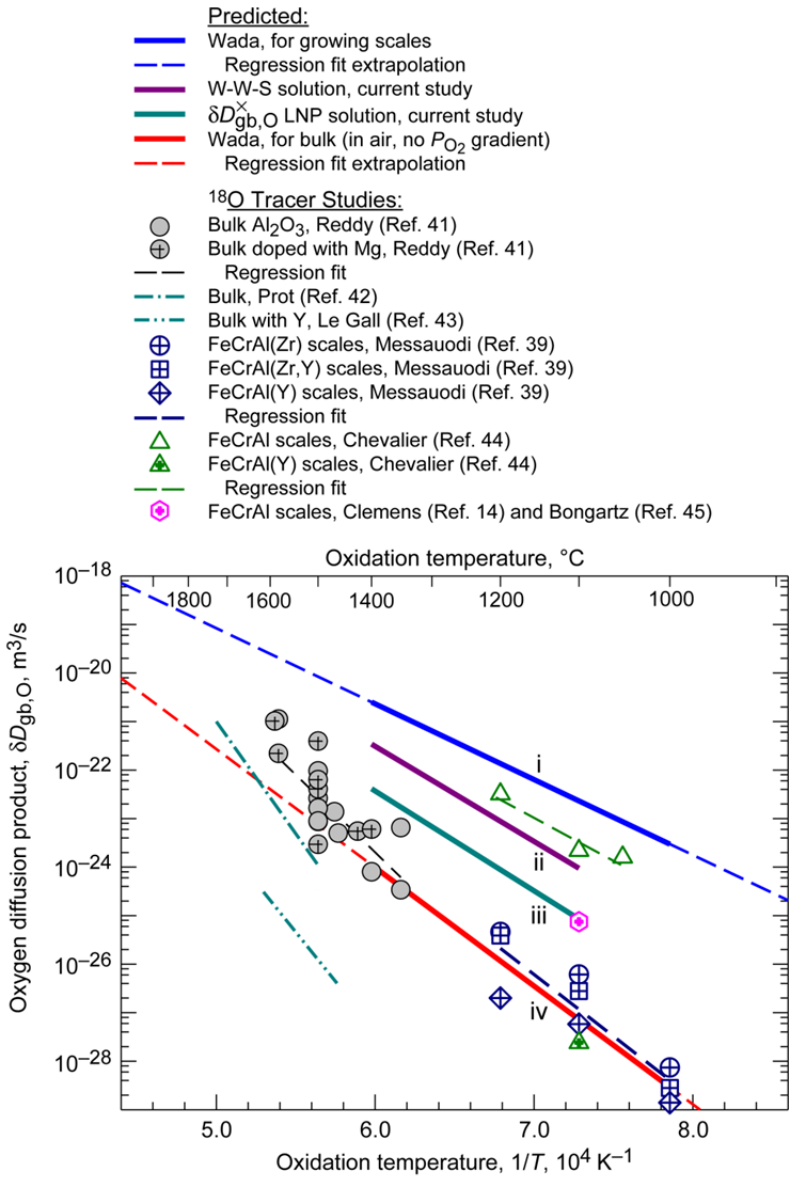

Figure 11.—Comparison of oxygen grain-boundary diffusion product $\delta D_{gb,O}$ calculated from four permeability relations (solid lines) to those measured from ^{18}O tracer profiles (dashed lines) in bulk Al_2O_3 and Al_2O_3 scales.

Finally, comparison is now made to more recent data for individual grain boundaries in bulk alumina (Fig. 12). The lower band (oriented) refers to bicrystal studies with varying habit planes and coincident site lattice Σ values (Ref. 46). The values for two Σ7 and Σ31 boundaries are quite close to those projected from the permeability relations for bulk alumina at atmospheric conditions, whereas the remaining curves are well below these. The upper cluster of points (random), recently obtained for individual grain boundaries in bulk polycrystalline (Ref. 47, personal communication), appears in a band with values near the projection of the W-W-S curve for scales. Since these represent boundaries where substantial tracer concentrations were observed, they may represent an upper band of diffusivities. In all, a variability of up to 8 orders of magnitude may be concluded from the bulk alumina data. Clearly, the nature of each grain boundary is of great importance and will enter into any discussion of alumina scale growth. At present, we can only assume that scale growth is controlled by some distribution of countless grain-boundary orientations, perhaps affected by growth textures in special cases.

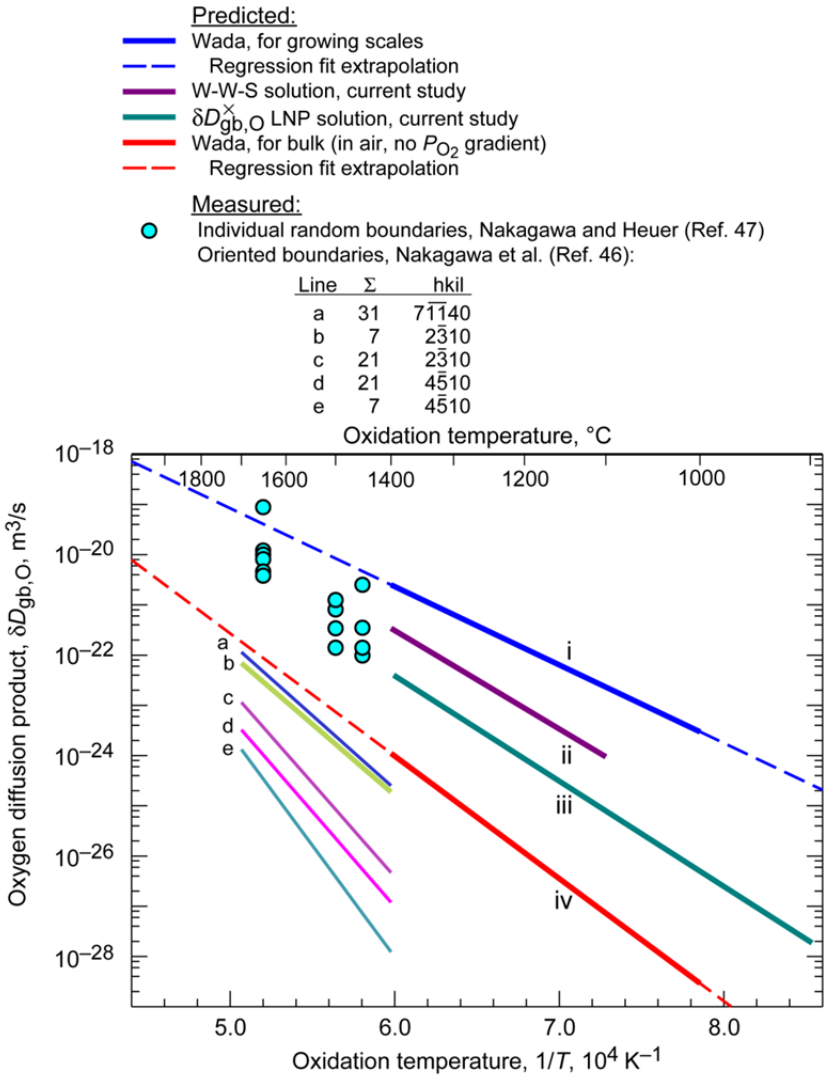

Figure 12.—Comparison of oxygen grain-boundary diffusion product $\delta D_{gb,O}$ for bulk Al_2O_3 and Al_2O_3 scales calculated from the four permeability relations (see Fig. 11) and those measured by ^{18}O tracer studies of individual grain boundaries: (1) Random boundaries measured by ToF-SIMS (time-of-flight secondary ion mass spectrometry) profiles of polycrystalline alumina (Nakagawa and Heuer, Ref. 47, personal communication) and (2) boundaries from bicrystals oriented by habit plane and tilt angle (Nakagawa et al., Ref. 46).

5.0 Activation Energies

A catalogue of activation energies obtained is presented in Table V. The top entry indicates the thermodynamic parameter resulting from an Arrhenius relation of the equilibrium P_{O_2} for the oxidation reaction (Fig. 2). The temperature dependence of the free energy of Al_2O_3 formation provides the dominant effect here. The next two values are those determined by Wada, Matsudaira, and Kitaoka (Ref. 24) for oxygen and aluminum boundary diffusion under atmospheric conditions, with P_{O_2} ~0.2 atm, independent of temperature (Fig. 2). The following two apply to the scale-metal interface (Table II and Fig. 2). It is seen that $Q_{int} = Q_{perm} + nQ_{eq}$, where Q_{int} is the activation energy resulting for diffusivity at the P_{O_2} calculated for the scale-metal interface, Q_{perm} is that provided from the permeability-derived diffusion relations (Eq. (1)), n is the exponent of the $P_{O_2}^n$ term in the latter, and Q_{eq} is that produced by the temperature dependence of $P_{O_2,eq}$. Thus, the activation energies for oxygen and aluminum diffusivity at the interface are reduced by 1/6 × (1012 kJ/mole) and increased by 3/16 × (1012 kJ/mole), respectively.

TABLE V.—ACTIVATION ENERGIES REPORTED FOR $\delta D_{gb,O}$ AND $\delta D_{gb,Al}$

[Calculated from permeability equations and estimated $\delta D_{gb,O}$ for FeCrAl(X) alloys using Wagner-Wada-Smialek (W-W-S) and $\Delta \ln P_{O_2}$ solutions.]

Source	Application	Value[a]	Activation energy, Q, kJ/mole	Reference
Thermodynamic	Al_2O_3 - FeCrAl	$P_{O_2,eq}$	1012	Jacobson (current study)
Wada	Bulk, scale (gas)	$\delta D_{gb,O}$	467	Wada (Ref. 24)
Wada	Bulk, scale (gas)	$\delta D_{gb,Al}$	604	Wada (Ref. 24)
Wagner-Wada	Scale, interface	$\delta D_{gb,O}$	298	Current study
Wagner-Wada	Scale, interface	$\delta D_{gb,Al}$	794	Current study
FeCrAl(Zr)	Scale (measured)	$k_{p,i}$	375	Current study
FeCrAl(Zr)	Scale (W-W-S)	$\delta D_{gb,O}$	375	Current study
FeCrAl(Zr)	Scale (LNP)	$\delta D_{gb,O}$	394	Current study
FeCrAl-Y_2O_3	Scale (W-W-S)	$\delta D_{gb,O}$	388	Ramanarayanan (Ref. 10)
FeCrAl-Y_2O_3	Scale (LNP)	$\delta D_{gb,O}$	294	Clemens (Refs. 13 and 14)
FeCrAlY	Scale (LNP)	$\delta D_{gb,O}$	321	Young (Ref. 12)
Ti_3AlC_2	Scale (LNP)	$\delta D_{gb,O}$	375	Wang (Ref. 32)
NiAl(Zr)	Scale (creep)	D_{gb}	434	Veal (Ref. 48)

[a] $P_{O_2,eq}$ is equilibrium oxygen pressure, δD_{gb} is grain-boundary diffusion product (for oxygen, O, and aluminum, Al), and D_{gb} is grain-boundary diffusivity.

The $k_{p,i}$ experimental data of the present study are given next and yield 375 kJ/mole. This is maintained in the Wagner-Wada-Smialek derivation of $\delta D_{gb,O}$, but changes to 394 kJ/mole in the $\Delta \ln P_{O_2}$ analysis, similar to 388 kJ/mole determined from the Ramanarayanan data. The last three list $\Delta \ln P_{O_2}$ results, giving 294, 321, and 375 kJ/mole for $\delta D_{gb,O}$ from oxidation of MA956, FeCrAlY, and Ti_3AlC_2, respectively. The first value (Ref. 14) may have been influenced by the high value at 900 °C; the next series (Ref. 12) was obtained from a narrow 100 °C temperature range, and the last (Ref. 32) is in closer agreement with the present study. All of these are substantially lower than the bulk alumina studies shown in Figure 11.

6.0 Additional Transport Issues

Up to this point the coupling of the permeability relations with oxidation kinetics has concentrated on oxygen grain-boundary diffusion in pure alumina. To some extent, this is all that is practical given that it is difficult to reliably separate any Al outward growth from primarily inward O growth. Furthermore, the study of dopant effects on diffusivity in bulk alumina is ongoing, with perhaps a tenuous connection to thermally grown scales with various grain-boundary dopant distributions.

6.1 Aluminum Diffusion

The importance of aluminum outward diffusion is often discussed in the literature, but it is not considered here given the detail required to cover just oxygen diffusion. For the sake of completeness, the same Wagner-type integrations were performed for the Wada relation for $\delta D_{\mathrm{gb,Al}}$ (Eq.(2)) and are listed in Appendix C. It is noteworthy that similar reduced terms result, allowing the Al diffusional component of k_p to be given as a simple function of $\delta D_{\mathrm{gb,Al,gas}}$ (Eq. (C4)), such that

$$k_{p,i,\mathrm{Al}} = \frac{16\ \delta D^{\text{W-W-S}}_{\mathrm{gb,Al,gas}}}{G_i} \tag{C4}$$

and the W-W-S expression is related to the LNP solution or average diffusivity by the factor 3/16 $\Delta \ln P_{\mathrm{O}_2}$. The difficulty, as with any system exhibiting mixed transport, is experimentally differentiating the minor Al contribution from that of oxygen to $k_{p,i}$ (Refs. 29 to 31).

We expect that the majority of transport is by oxygen diffusion, as controlled by the interface P_{O_2}, such that oxygen diffusivity at the interface is 2 to 5 orders of magnitude greater than aluminum at the gas surface, the largest differential being at lower temperature. Furthermore in the modeled case of oxidation at 1100 °C, Al diffusivity is seen to be negligible except at the outermost near surface of the scale (Fig. 10 in Ref. 18). Thus the focus on oxygen diffusivity in the present study is consistent with the permeability projections.

6.2 Dopant Effects

It must be acknowledged that Al transport is a key factor in explaining growth stress and the formation of oxide within the scale or at outer grain-boundary ridges. The effects of impurities or intentional dopants often enter this conversation, as in producing charge compensating defects that may affect Al diffusion. Although, again, not the focus of the present study, the permeability experiments performed on Lu-, Y-, and Hf-doped alumina addressed these issues, reaching P_{O_2} down to 10^{-8} Pa (Refs. 17, 18, and 49). It was found in general that Lu and Y dopants (on the order of 0.4 at.% Lu_2O_3) reduced oxygen grain-boundary diffusivity by about 3 times, with no change in aluminum diffusivity, whereas Hf dopants (0.2% HfO_2) reduced Al diffusivity by about 2 times, with no change in oxygen diffusivity. This is supported by an order of magnitude reduction in oxygen diffusivity for an Y-doped bicrystal found in tracer studies (Ref. 50). Surprisingly, co-doping with equal amounts of Lu and Y produced about a 1.5-times increase in both Al and O diffusivity in the permeability studies (Ref. 18). These results support the often-observed beneficial effect of Hf dopants on alumina scale growth, but do not completely resolve effects typically reported for optimum Y-doping or co-doping where Al diffusivity and outward growth appear to be reduced. In the present study, it may be expected that some of the 10 to 40 times lower offset of oxidation-derived values in comparison to permeability predictions (Figs. 7, 9, and 10) are due to dopant effects. In this work and the Messaoudi data (Ref. 36), the dopant was Zr and may be expected to exhibit effects similar to those of Hf. However, examination of these figures shows that the data for Zr, Y, Ti, and Y_2O_3 dopants all agree with nearly a single Arrhenius relationship. Thus

clear discrimination of oxidation kinetics by dopant type, to the extent suggested by the permeability studies, has not emerged.

There has been much discussion of various effects of Y-doping (or other reactive elements). Initially reduced Al transport, growth stress, and buckling occur as Y levels increase and then give way to increased weight gains and disruptions from oxidation of Y-rich precipitates (e.g., YAG, yttrium aluminum garnet) and oxide intrusions. Finally, Hf dopants are recognized as perhaps the most effective in reducing k_p, by about an order of magnitude, and receive a great deal of attention in protective commercial Hf-modified MCrAlY overlay or NiAl diffusion coatings (Ref. 4). There does not yet seem to be an exact correlation between dopant effects on oxidation with those predicted by the permeability studies.

It is acknowledged that 10 to 100 ppm of common Ni, Co, Fe, Cr, and Si base metal impurities may be present in alumina scales grown on typical alloys. A comparison of reactive element dopant effects in bulk aluminas containing these metals may thus provide further insight if data from a "pure" alumina scale were analyzed, such as that formed on Pt-Al alloys.

6.3 Π Decay for FeCrAl(Zr)

According to Equation (10) the oxidation product $\Pi = k_{p,i} \cdot G_i$ should be a constant and equal to 12 $\delta D_{\mathrm{gb,O}}$. This was indeed the case for the 1200 °C FeCrAlY data in Figure 8 (Ref. 35), even out to 2000 h. However, the present study suggests an accelerating decrease in this term after about 200 h. One potential cause might be reduced grain-boundary diffusion according to Equation (10). Although there is no evidence either way, significant Al depletion would reduce the interfacial Al activity and increase $P_{\mathrm{O_2,eq}}$ according to Equation (14). Then an increase in $P_{\mathrm{O_2}}$ would result in a decrease in $\delta D_{\mathrm{gb,O}}$ according to Equation (1). Since the Al content and thickness of the Naumenko samples were less than the present FeCrAl(Zr) alloy, it cannot be argued that greater Al depletion from a reduced Al reservoir resulted in the present study. Nor was greater spallation observed. At present there is no compelling explanation for the long-term decay in the oxidation product, Π.

7.0 Summary and Concluding Remarks

The temperature and pressure dependence of oxygen and aluminum grain-boundary diffusivity were determined by permeability studies of pure bulk alumina wafers by Wada, Matsudaira, and Kitaoka in 2011. Their work is extended in the present study to further elucidate the growth kinetics of high-temperature alumina scales as a function of grain-boundary diffusivity, δD_{gb}. First, equilibrium thermodynamics was applied to the case of a commercial FeCrAl alloy to determine the equilibrium oxygen pressure at the metal interface $P_{\mathrm{O_2,int,eq}}$. These values and the permeability relations were applied to a modified Wagner equation for ionic scales. For growth primarily by oxygen grain-boundary diffusion, the following relation was developed (Eq. (18)) for the instantaneous parabolic rate constant (at a grain size of 0.5 μm):

$$k_{p,i}\,[\mathrm{W\text{-}W\text{-}S}] = 1.24\times10^{-4}\exp\left(\frac{-298\,\mathrm{kJ}}{RT}\right)\ \mathrm{m^2/s}$$

This is compared to a relation determined experimentally (exptl) for the same scales (Eq. (16)), with a moderately higher activation energy:

$$k_{p,i,\mathrm{exptl}} = 4.29\times10^{-3}\exp\left(\frac{-375\,\mathrm{kJ}}{RT}\right)\ \mathrm{m^2/s}$$

It is also found that a grain-size invariant oxidation rate product, $\Pi = k_{p,i} \cdot G_i$ is a simple function of oxygen grain-boundary diffusivity from a Wagner-Wada-Smialek (W-W-S) derivation. Thus, from Equation (10),

$$\Pi_i = k_{p,i} G_i = 12 \delta D_{\mathrm{gb,O,int}}$$

here δD_{gb} is a strong function of P_{O_2} and varies across the scale. This provides a surprisingly convenient means of drawing comparisons: it allows either prediction of oxidation rates from independently measured diffusivity or prediction of grain-boundary diffusivity from instantaneous oxidation rate and grain size. As simple as this relation appears, the real complexity of transport issues are embedded in the starting permeability relations, the Wagner integral, and the Hart/Smeltzer diffusivity equations.

Comparisons to similar oxidation studies yielded relative overall agreement, confirming some level of confidence in the experimental data and the concept of an invariant oxidation constant, Π. The predicted oxidation kinetics trended from ~10 to 40 times greater than the experimental values as temperature was reduced. Although this is not exact agreement, it is enormously closer than extrapolations of bulk alumina diffusivity studies obtained with no P_{O_2} gradient. Moreover, the discrepancy may be partially ascribed to the experimental data pertaining to doped alumina scales, whereas the predicted data are for pure alumina.

For the sake of completeness, comparisons were made to predictions where constant (average) diffusivity was assumed across the scale. Here a standard correction factor, $\left(\Delta \ln P_{\mathrm{O}_2}\right) / 6$ could be applied to obtain $k_{p,i}$ from the comparable W-W-S expression or the inverse factor for obtaining diffusivity from the experimental $k_{p,i}$. Also, the extremes of aluminum and oxygen diffusivity were explored at each interface, and $\delta D_{\mathrm{gb,Al}}$ was found to be negligible compared to $\delta D_{\mathrm{gb,O}}$, except at the gas surface. Though not utilized here, an analogous method resulted in a simplified W-W-S relation for $\delta D_{\mathrm{gb,Al}}$, which can just be added to the oxygen contribution for a full solution to the Wagner integral (Eq. (B4)):

$$k_{p,i,\mathrm{Al}} G_i = 16 \delta D_{\mathrm{gb,Al,gas}}^{\mathrm{W\text{-}W\text{-}S}}$$

In all, the permeability studies, by quantifying P_{O_2} effects on grain-boundary diffusivity, have allowed for improved insights and closer connections between predicted diffusivity and alumina scale growth kinetics.

Appendix A.—Symbols

Symbols:

A	pre-exponential exponent from Equation (9)
a	activity
D	diffusivity
f	area fraction of short-circuit grain-boundary paths
G	grain size (diameter)
k	oxidation rate constant
K	equilibrium constant
P	pressure
Q	activation energy
R	ideal gas constant
r^2	correlation coefficient
T	temperature
t	time
x	scale weight gain, or equivalent thickness
z	ionic charge
δ	grain-boundary width
Π	oxidation product

Subscripts:

0.5	0.5-μm grain size
I	low-P_{O_2} surface
II	high-P_{O_2} surface
a	anion
Al	aluminum
c	cation
eff	effective
eq	equilibrium
exptl	experimental
gas	gas
gb	grain boundary
i	instantaneous
int	interface
L	lattice
m	grain growth time exponent
n	oxidation time exponent
O	oxygen
O_2	oxygen gas
p	parabolic
perm	permeability

Appendix B.—Defect Equilibria, Electroneutrality, and P_{O_2}

The oxidation reaction and basic defect equilibria for undoped alumina can be described by Equations (B1) to (B5) using Kröger-Vink notation (Ref. 23). Equations (B2) and (B4) apply to the oxygen vacancy concentration $\left[V_O^{\bullet\bullet}\right]$ at the low-P_{O_2} surface (n-type), and Equations (B3) and (B5) apply to the aluminum vacancy concentration $\left[V_{Al}'''\right]$ at the high-P_{O_2} surface (p-type). The equilibrium constants are then written as Equations (B6) to (B8), corresponding to Equations (B1) to (B3). Solving the electroneutrality relations Equations (B4) and (B5) for $[V_i]$ and substituting into the corresponding equilibrium relations Equations (B7) and (B8) produce Equations (B9) and (B11), respectively. Finally, combining Equation (B1) with (B9) produces Equation (B10). Thus, at the low-P_{O_2} surface $\left[V_O^{\bullet\bullet}\right]$ is proportional to $P_{O_2}^{-1/6}$, and at the high P_{O_2} surface $\left[V_O'''\right]$ is proportional to $P_{O_2}^{3/16}$.

$$2Al + \tfrac{3}{2}O_2 = Al_2O_3 \tag{B1}$$

$$2Al = 2Al_{Al}^{\otimes} + 3V_O^{\bullet\bullet} + 6e' \text{ (n - type)} \tag{B2}$$

$$\tfrac{3}{2}O_2 = 3O_O^{\otimes} + 2V_{Al}''' + 6h^{\bullet} \text{ (p - type)} \tag{B3}$$

$$2\left[V_O^{\bullet\bullet}\right] = [e'] \tag{B4}$$

$$3\left[V_{Al}'''\right] = \left[h^{\bullet}\right] \tag{B5}$$

$$K_1 = \frac{1}{a_{Al}^2 P_{O_2}^{3/2}} \tag{B6}$$

$$K_2 = \frac{1^2\left[V_O^{\bullet\bullet}\right]^3[e']^6}{a_{Al}^2} \tag{B7}$$

$$K_3 = \frac{1^3\left[V_{Al}'''\right]^2\left[h^{\bullet}\right]^6}{P_{O_2}^{3/2}} \tag{B8}$$

$$K_2 = \frac{2^6\left[V_O^{\bullet\bullet}\right]^9}{a_{Al}^2} \tag{B9}$$

$$\left[V_O^{\bullet\bullet}\right] = 2^{-2/3}\left(\frac{K_2}{K_1}\right)^{1/9} P_{O_2}^{-1/6} \tag{B10}$$

$$\left[V_{Al}'''\right] = 3^{-3/4} K_3^{1/8} P_{O_2}^{+3/16} \tag{B11}$$

Appendix C.—Relations Derived for Aluminum Grain-Boundary Diffusivity, $\delta D_{gb,Al}$

The complete Wagner expression for alumina growth by aluminum and oxygen diffusion is obtained from Equation (4) as

$$k_{p,i} = 2x\frac{\mathrm{d}x}{\mathrm{d}t} = \int_{P_{O_2,\mathrm{int}}}^{P_{O_2,\mathrm{gas}}} \left(\tfrac{3}{2} D_{\mathrm{eff,Al}} + D_{\mathrm{eff,O}}\right) \mathrm{d}\ln P_{O_2} \tag{C1}$$

Dealing again only with one component, the aluminum contribution, obtained from Equation (2) (repeated here):

$$\delta D_{\mathrm{gb,Al}} = 2.475\times10^{-5} \exp\left(\frac{-604\ \mathrm{kJ}}{RT}\right) P_{O_2,\mathrm{II}}^{+3/16}$$

produces the following form, Equation (C2), integrated to Equation (C3) (Wagner-Wada-Smialek, W-W-S) and simplified to Equation (C4) (and (C5) if a constant $D^{\times}_{\mathrm{gb,Al}}$ is assumed). Finally, the relationship between the W-W-S and LNP solutions for $\delta D_{\mathrm{gb,Al}}$ are given by Equation (C6):

$$k_{p,i,\mathrm{Al}} = \int_{P_{O_2,\mathrm{int}}}^{P_{O_2,\mathrm{gas}}} \tfrac{3}{2} \frac{2\delta D_{\mathrm{gb,Al}}}{G_i} \mathrm{d}\ln P \tag{C2}$$

$$k_{p,i,\mathrm{Al}} = \frac{A_2 \exp\left(-Q_2/RT\right)}{G_i} 16\Delta P_{O_2}^{+3/16} \tag{C3}$$

$$k_{p,i,\mathrm{Al}} = \frac{16\delta D^{\text{W-W-S}}_{\mathrm{gb,Al,gas}}}{G_i} \tag{C4}$$

$$k_{p,i,\mathrm{Al}} = \frac{3\delta D^{\times}_{\mathrm{gb,Al}}}{G_i} \Delta\ln P_{O_2} \tag{C5}$$

$$\delta D^{\text{W-W-S}}_{\mathrm{gb,Al,gas}} = \frac{3\Delta\ln P_{O_2}}{16} \delta D^{\times}_{\mathrm{gb,Al}} \tag{C6}$$

References

1. Hindam, H.; and Whittle, D.P.: Microstructure, Adhesion and Growth Kinetics of Protective Scales on Metals and Alloys. Oxid. Met., vol. 18, nos. 5–6, 1982, pp. 245–284.
2. Hou, Peggy Y.: Impurity Effects on Alumina Scale Growth. J. Am. Ceram. Soc., vol. 86, no. 4, 2003, pp. 660–668.
3. Stott, F. Howard: The Oxidation of Alumina-Forming Alloys. High Temperature Corrosion and Protection of Materials 4, vols. 1 and 2, 1997, pp. 19–32.
4. Pint, B.A.: High Temperature Corrosion of Alumina-Forming Iron, Nickel and Cobalt-Base Alloys. Schreir's Corrosion, Fourth ed., vol. 1, 2010, pp. 606–645.
5. Huntz, A.M., et al.: Diffusion Studies in Oxides Scales Grown on Alumina- and Chromia-Forming Alloys. Scr. Mater., vol. 37, no. 5, 1997, pp. 651–660.
6. Balmain, J.; Loudjani, M.K.; and Huntz, A.M.: Influence of Yttrium on Transport Properties of α Alumina Scales Developed on Yttrium Implanted β NiAl. Radiat. Eff. Defects Solids, vol. 137, nos. 1–4, 1995, pp. 291–294.
7. Balmain, J.; and Huntz, A.M.: Improvement of the Application of an Electrochemical Method for the Determination of Transport Properties of an Alumina Scale. Part I: Alumina Scale on a β-NiAl Alloy. Oxid. Met., vol. 45 nos. 1–2, 1996, pp. 183–196.
8. Balmain, J.; and Huntz, A.M.: Improvement of the Application of an Electrochemical Method for the Determination of Transport Properties of an Alpha-Alumina Scale. Part II: Influence of Yttrium and Palladium on Alumina Scales Developed on a β-NiAl Alloy. Oxid. Met., vol. 46, nos. 3–4, 1996, pp. 213–234.
9. Balmain, J.; Huntz, A.M.; and Philibert, J.: Atomic Transport Properties in Alumina Scales and Calculation of the Oxidation Parabolic Rate Constant. Defect and Diffusion Forum, vol. 143, no. 2, 1997, pp. 1189–1194.
10. Ramanarayanan, T.A.; Raghavan, M.; and Petkovic-Luton, R.: The Characteristics of Alumina Scales Formed on Fe-Based Yttria-Dispersed Alloys. J. Electrochem. Soc., vol. 131, no. 4, 1984, pp. 923–931.
11. Balmain, J.; Loudjani, M.K.; and Huntz, A.M.: Microstructural and Diffusional Aspects of the Growth of Alumina Scales on β-NiAl. Mater. Sci. Eng., A, vol. 224, nos. 1–2, 1997, pp. 87–100.
12. Young, D.J., et al.: Oxidation Kinetics of Y-Doped FeCrAl-Alloys in Low and High pO_2 Gases. Mater. Corros., vol. 61, no. 10, 2010, pp. 838–844.
13. Clemens, D., et al.: Analysis and Modelling of Transport Processes in Alumina Scales on High-Temperature Alloys. Fresen. J. Anal. Chem., vol. 346, nos. 1–3, 1993, pp. 318–322.
14. Clemens, D., et al.: Determination of Lattice and Grain-Boundary Diffusion Coefficients in Protective Alumina Scales on High Temperature Alloys Using SEM, TEM and SIMS. Fresen. J. Anal. Chem., vol. 353, nos. 3–4, 1995, pp. 267–270.
15. Chatterjee, A., et al.: Kinetic Modeling of High Temperature Oxidation of Ni-Base Alloys. Comput. Mater. Sci., vol. 50 no. 3, 2011, pp. 811–819.
16. Kitaoka, Satoshi; Matsudaira, Tsuneaki; and Wada, Masashi: Mass-Transfer Mechanism of Alumina Ceramics Under Oxygen Potential Gradients at High Temperatures. Mater. Trans., JIM, vol. 50, no. 5, 2009, pp. 1023–1031.
17. Matsudaira, Tsuneaki, et al.: The Effect of Lutetium Dopant on Oxygen Permeability of Alumina Polycrystals Under Oxygen Potential Gradients at Ultra-High Temperatures. Acta Mater., vol. 58, no. 5, 2010, pp. 1544–1553.
18. Matsudaira, Tsuneaki, et al.: Oxygen Permeability in Cation-Doped Polycrystalline Alumina Under Oxygen Potential Gradients at High Temperatures. Acta Mater., vol. 59, no. 14, 2011, pp. 5440–5450.
19. Matsudaira, Tsuneaki, et al.: Mass Transfer Through a Single Grain-Boundary in Alumina Bicrystals Under Oxygen Potential Gradients. J. Mater. Sci., vol. 46, 2011, pp. 4407–4412.

20. Smialek, J.L.: Microstructure of Al_2O_3 Scales Formed on NiCrAl Alloys; Ph.D. Thesis; Case Western Reserve Univ., NASA TM–81676, 1981.
21. Smialek, J.L.; and Gibala, R.: Diffusion Processes in Al_2O_3 Scales—Void Growth, Grain Growth, and Scale Growth. High Temperature Corrosion. Proceedings of the International Conference, San Diego, CA, 1983, pp. 274–283.
22. Heuer, Arthur H., et al.: Alumina Scale Formation: A New Perspective. J. Am. Ceram. Soc., vol. 94, no. S1, 2011, pp. S146–S153.
23. Kofstad, Per: High Temperature Corrosion. Elsevier, London, 1988.
24. Wada, Masashi; Matsudaira, Tsuneaki; and Kitaoka, Satoshi: Mutual Grain-Boundary Transport of Aluminum and Oxygen in Polycrystalline Al_2O_3 Under Oxygen Potential Gradients at High Temperatures. J. Ceram. Soc. Jpn., vol. 119, no. 11, 2011, pp. 832–839.
25. Hindam, H.M.; and Smeltzer, W.W.: Growth and Microstructure of α-Al_2O_3 on β-NiAl Alloys. J. Electrochem. Soc., vol. 127, no. 7, 1980, pp. 1630–1635.
26. Hart, E.W.: On the Role of Dislocations in Bulk Diffusion. Acta Metall., vol. 5, 1957, p. 597.
27. Smeltzer, W.W.; Haering, R.R.; and Kirkaldy, J.S.: Oxidation of Metals By Short Circuit and Lattice Diffusion of Oxygen. Acta Metall., vol. 9, 1961, p. 880.
28. Doychak, J.; Smialek, J.L.; and Mitchell, T.E.: Transient Oxidation of Single-Crystal β-NiAl. Metall. Trans. A, vol. 20, no. 3, 1989, pp. 499–518.
29. Nychka, J.A.; and Clarke, D.R.: Quantification of Aluminum Outward Diffusion During Oxidation of FeCrAl Alloys. Oxid. Met., vol. 63, nos. 5–6, 2005, pp. 325–352.
30. Prescott, R., et al.: Oxidation Mechanisms of β-NiAl+Zr Determined by SIMS. Corros. Sci., vol. 37, no. 9, 1995, pp. 1341–1364.
31. Tolpygo, V.K.; and Clarke, D.R.: Microstructural Evidence for Counter-Diffusion of Aluminum and Oxygen During the Growth of Alumina Scales. Mater. High Temp., vol. 20, no. 3, 2003, pp. 261–271.
32. Wang, X.H., et al.: Insights Into High Temperature Oxidation of Al_2O_3-Forming Ti_3AlC_2. Corros. Sci., vol. 58, 2012, pp. 95–103.
33. CompuTherm LLC: PandatTM. 2008. http://www.computherm.com/index.php?route=product/category&path=71 Accessed April 19, 2013.
34. ThermFact Inc. and GTT-Technologies: FactSage 6.3. http://www.factsage.com/ Accessed April 19, 2013.
35. Naumenko, D., et al.: Correlation Between the Microstructure, Growth Mechanism, and Growth Kinetics of Alumina Scales on a FeCrAlY Alloy. Metall. Mater. Trans. A, vol. 38A, no. 12, 2007, pp. 2974–2983.
36. Messaoudi, K.; Huntz, A.M.; and Lesage, B.: Diffusion and Growth Mechanism of Al_2O_3 Scales on Ferritic Fe-Cr-Al Alloys. Mater. Sci. Eng., A, vol. A247, 1998, pp. 248–262.
37. Tolpygo, V.: Grain Growth Effects on Alumina Scale Kinetics. Presented at the High Temperature Corrosion and Protection of Materials Conference, P. Steinmetz et al., eds., les Embiez, France, 2008.
38. Quadakkers, W.J.: Growth Mechanisms of Oxide Scales on ODS Alloys in the Temperature Range 1000–1100 °C. Mater. Corros., vol. 41, no. 12, 1990, pp. 659–668.
39. Quadakkers, W.J., et al.: Growth Rates of Alumina Scales on Fe-Cr-Al Alloys. Oxid. Met., vol. 61, nos. 1–2, 2004, pp. 17–37.
40. Heuer, A.H.: Oxygen and Aluminum Diffusion in α-Al_2O_3: How Much Do We Really Understand? J. Eur. Ceram. Soc., vol. 28, no. 7, 2008, pp. 1495–1507.
41. Reddy, K. Pattabhi Rami: Oxygen Diffusion in Close Packed Oxides. Ph.D. Thesis, Case Western Reserve Univ., 1979.
42. Prot, D., et al.: Self-Diffusion in α-Al_2O_3. IV. Oxygen Grain-Boundary Self-Diffusion in Undoped and Yttria-Doped Alumina Polycrystals. Philos. Mag. A, vol. 73, no. 4, 1996, pp. 935–949.
43. Le Gall, M., et al.: Oxygen Self-Diffusion in Y_2O_3 Doped α Alumina. Mater. Sci. Forum, vols. 126–128, 1993, pp. 411–414.

44. Chevalier, S., et al.: Oxygen Diffusion in Alumina. Application to Synthetic and Thermally Grown Al_2O_3. Defect and Diffusion Forum, vols. 237–240, 2005, pp. 899–910.
45. Bongartz, K., et al.: Mathematical Modeling of Oxide Growth Mechanisms Measured by 18O Tracer Experiments. Surf. Sci., vol. 292, nos. 1–2, 1993, pp. 196–208.
46. Nakagawa, Tsubasa, et al.: Grain Boundary Character Dependence of Oxygen Grain-Boundary Diffusion in α-Al_2O_3 Bicrystals. Scr. Mater., vol. 65, no. 6, 2011, pp. 544–547.
47. Nakagawa, T.; and Heuer, A.H.: Case Western Reserve University, Cleveland, OH, personal communication, 2012.
48. Veal, B.W.; and Paulikas, A.P.: Growth Strains and Creep in Thermally Grown Alumina: Oxide Growth Mechanisms. J. Appl. Phys., vol. 104, no. 9, 2008.
49. Kitaoka, Satoshi; Matsudaira, Tsuneaki; and Wada, Masashi: Effect of Dopants on Interdiffusion of Aluminum and Oxygen Through Grain-Boundaries in Polycrystalline Alumina. International Symposium on Defects, Transport and Related Phenomena, Pittsburgh, PA, 2012.
50. Nakagawa, T., et al.: Oxygen Diffusion Blocking of Single Grain-Boundary in Yttria-Doped Zirconia Bicrystals. J. Mater. Sci., vol. 40, no. 12, 2005, pp. 3185–3190.

REPORT DOCUMENTATION PAGE	Form Approved OMB No. 0704-0188

1. REPORT DATE *(DD-MM-YYYY)*	2. REPORT TYPE	3. DATES COVERED *(From - To)*
01-08-2013	Technical Memorandum	

4. TITLE AND SUBTITLE
Oxygen Permeability and Grain-Boundary Diffusion Applied to Alumina Scales

5a. CONTRACT NUMBER

5b. GRANT NUMBER

5c. PROGRAM ELEMENT NUMBER

6. AUTHOR(S)
Smialek, James, L.; Jacobson, Nathan, S.; Gleeson, Brian; Hovis, David, B.; Heuer, Arthur, H.

5d. PROJECT NUMBER

5e. TASK NUMBER

5f. WORK UNIT NUMBER
WBS 473452.02.03.05.04.01.01

7. PERFORMING ORGANIZATION NAME(S) AND ADDRESS(ES)
National Aeronautics and Space Administration
John H. Glenn Research Center at Lewis Field
Cleveland, Ohio 44135-3191

8. PERFORMING ORGANIZATION REPORT NUMBER
E-18644

9. SPONSORING/MONITORING AGENCY NAME(S) AND ADDRESS(ES)
National Aeronautics and Space Administration
Washington, DC 20546-0001

10. SPONSORING/MONITOR'S ACRONYM(S)
NASA

11. SPONSORING/MONITORING REPORT NUMBER
NASA/TM-2013-217855

12. DISTRIBUTION/AVAILABILITY STATEMENT
Unclassified-Unlimited
Subject Category: 01
Available electronically at http://www.sti.nasa.gov
This publication is available from the NASA Center for AeroSpace Information, 443-757-5802

13. SUPPLEMENTARY NOTES

14. ABSTRACT
High-temperature oxygen permeability measurements had determined grain-boundary diffusivities (δD_{gb}) in bulk polycrystalline alumina (Wada, Matsudaira, and Kitaoka). They predict that oxygen $\delta D_{gb,O}$ varies with oxygen pressure as $P(O_2)^{-1/6}$ at low pressure whereas aluminum $\delta D_{gb,Al}$ varies with $P(O_2)^{+3/16}$ at high pressure. These relations were used to evaluate alumina scale growth in terms of diffusivity and grain size. A modified Wagner treatment for dominant inward oxygen growth produces the concise solution: $\Pi_i = k_{p,i} \times G_i = 12\ \delta D_{gb,O,int}$, where Π_i is a constant and $k_{p,i}$ and G_i refer to instantaneous values of the scale parabolic growth constant and grain size, respectively. A commercial FeCrAl(Zr) alloy was oxidized at 1100 to 1400 °C to determine $k_{p,i}$, interfacial grain size, Π, and thus $\delta D_{gb,O,int}$. The $\delta D_{gb,O,int}$ values predicted from oxidation at (375 kJ/mole) were about 20 times less than those obtained above (at 298 kJ/mole), but closer than extrapolations from high-temperature bulk measurements. The experimental oxidation results agree with similar FeCrAl(X) studies, especially where both $k_{p,i}$ and G_i were characterized. This complete approach accounts for temperature-sensitive oxidation effects of grain enlargement, equilibrium interface pressure variation, and grain-boundary diffusivity.

15. SUBJECT TERMS
High-temperature alloys; Oxide scales; Diffusion

16. SECURITY CLASSIFICATION OF:			17. LIMITATION OF ABSTRACT	18. NUMBER OF PAGES	19a. NAME OF RESPONSIBLE PERSON
a. REPORT	b. ABSTRACT	c. THIS PAGE			STI Help Desk (email:help@sti.nasa.gov)
U	U	U	UU	42	19b. TELEPHONE NUMBER *(include area code)* 443-757-5802